Journal of Medicinal Chemistry

Article

pubs.acs.org/jmc

Development of Highly Potent and Selective Diaminothiazole Inhibitors of Cyclin-Dependent Kinases

Ernst Schonbrunn,*[,†] Stephane Betzi,[†] Riazul Alam,[†] Mathew P. Martin,[†] Andreas Becker,[†] Huijong Han,[†] Rawle Francis,[‡] Ramappa Chakrasali,[‡] Sudhakar Jakkaraj,[‡] Aslamuzzaman Kazi,[†] Said M. Sebti,[†] Christopher L. Cubitt,[§] Anthony W. Gebhard,[∥] Lori A. Hazlehurst,[∥] Joseph S. Tash,[⊥] and Gunda I. Georg*[,‡]

[†]Drug Discovery Department, H. Lee Moffitt Cancer Center and Research Institute, 12902 Magnolia Drive, Tampa, Florida 33612, United States

[‡]Department of Medicinal Chemistry, Institute for Therapeutics Discovery and Development, University of Minnesota, 717 Delaware Street SE, Minneapolis, Minnesota 55414, United States

[§]Translational Research Laboratory, H. Lee Moffitt Cancer Center and Research Institute, 12902 Magnolia Drive, Tampa, Florida 33612, United States

[∥]Molecular Oncology Department, H. Lee Moffitt Cancer Center and Research Institute, 12902 Magnolia Drive, Tampa, Florida 33612, United States

[⊥]Department of Molecular and Integrative Physiology, University of Kansas Medical Center, 3901 Rainbow Boulevard, Kansas City, Kansas 66160, United States

Supporting Information

ABSTRACT: Cyclin-dependent kinases (CDKs) are serine/threonine protein kinases that act as key regulatory elements in cell cycle progression. We describe the development of highly potent diaminothiazole inhibitors of CDK2 (IC_{50} = 0.0009−0.0015 μM) from a single hit compound with weak inhibitory activity (IC_{50} = 15 μM), discovered by high-throughput screening. Structure-based design was performed using 35 cocrystal structures of CDK2 liganded with distinct analogues of the parent compound. The profiling of compound **51** against a panel of 339 kinases revealed high selectivity for CDKs, with preference for CDK2 and CDK5 over CDK9, CDK1, CDK4, and CDK6. Compound **51** inhibited the proliferation of 13 out of 15 cancer cell lines with IC_{50} values between 0.27 and 6.9 μM, which correlated with the complete suppression of retinoblastoma phosphorylation and the onset of apoptosis. Combined, the results demonstrate the potential of this new inhibitors series for further development into CDK-specific chemical probes or therapeutics.

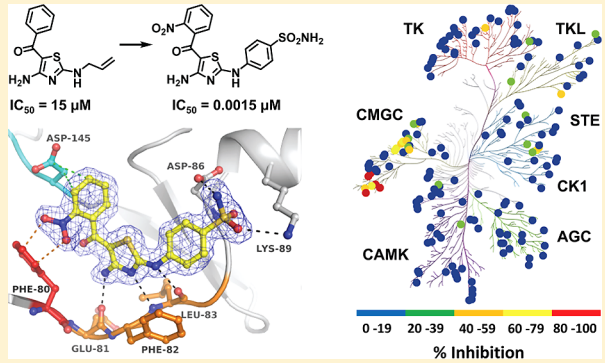

INTRODUCTION

Protein kinases have been implicated in a myriad of human diseases, including various cancers and neurodegenerative disorders. Cyclin-dependent kinases (CDKs) are a family of serine/threonine kinases that are involved in cell cycle progression and transcription. Deregulation of CDKs has been associated with a number of medical conditions, and they have therefore become validated and important targets in drug discovery.[1,2] The functionality of CDKs is dependent on specific interactions with regulatory partner proteins, the cyclins.[3−5] Cell-cycle progression depends on the activity of CDK1, CDK2, CDK4, and CDK6. CDK4/6 in complex with cyclin D1, D2, or D3 and CDK2 in complex with cyclin E promote S-phase entry by phosphorylating and inactivating the retinoblastoma (Rb) protein. CDK2-cyclin A and CDK1-cyclin A propel cells through the S-phase, and CDK1-cyclin B is responsible for mitosis.[6,7] CDK-specific inhibitors induce apoptosis by repressing transcription and/or by perturbing the cell cycle.[8] As alterations in checkpoint regulation can lead to aberrant cell division, CDK2 represents an attractive target for therapeutics designed to arrest or recover control of the cell cycle.[9,10] Additionally, CDK2 is essential for completion of prophase I during meiotic cell division in male and female germ cells, and CDK2−/− knockout mice are viable but sterile.[11−13] Therefore, CDK2 also provides promise as a target for the development of nonhormonal male contraceptive agents that do not exhibit the significant side effects associated with hormone-based agents currently available for female contraception and under development for male contraception.[14−16]

Received: August 27, 2012
Published: April 19, 2013

Several CDK inhibitors have been in clinical development since the 1990s. These first-generation inhibitors, namely flavopiridol, (*R*)-roscovitine, SNS-032,[17] and PHA-793887,[18] were discontinued during phase II or phase III trials due to unfavorable pharmacological properties and low specificity resulting in undesirable off-target interactions. Recently, two new-generation CDK inhibitors, dinaciclib (Merck, SCH727965) and palbociclib (Pfizer, PD-0332991), advanced to phase III trials for refractory chronic lymphocytic leukemia and advanced estrogen receptor (ER)-positive breast cancer, respectively.[19,20] Dinaciclib is a selective inhibitor of CDK1, CDK2, CDK5, and CDK9,[21,22] while palbociclib is a selective inhibitor of CDK4 and CDK6.[23]

In an attempt to discover new CDK2 inhibitors with promising scaffolds for hit-to-lead development, we screened 103000 compounds from commercial libraries against the human CDK2-cyclin A2 complex. Hit compound 2-(allylamino)-4-aminothiazol-5-yl)(phenyl)methanone (**1**) was selected for thorough structure–activity relationship (SAR) analysis using medicinal chemistry and protein crystallography, yielding compounds with high potency and selectivity against CDK2 and CDK5 over CDK9, CDK1, CDK4, and CDK6. Compound **51** inhibited the proliferation/survival of five cancer cell lines with IC_{50} values ≤ 0.5 μM, suppressed CDK-specific phosphorylation of the Rb protein, and induced activation of caspase-3. The comprehensiveness of this experimental structure–activity data, including 35 cocrystal structures of CDK2 with analogues of the parent compound, provides valuable guidance for the refinement of algorithms used in molecular docking simulations and structure-based drug design.

RESULTS AND DISCUSSION

HTS Hit Identification and Characterization. We discovered compound **1** (2-(allylamino)-4-aminothiazol-5-yl-(phenyl)methanone) by high-throughput screening (HTS) as an inhibitor of the human CDK2-cyclin A2 complex with an IC_{50} value of 15 μM. The cocrystal structure with CDK2 at 1.85 Å resolution (Figure 1, Table S1 in Supporting Information) confirmed that **1** belongs to the type I class of kinase inhibitors, binding to the ATP site through hydrogen bonding interactions between the thiazolamine moiety and the hinge region (Glu81–Leu83). A water molecule bridges the carbonyl oxygen of **1** and the backbone amide nitrogen of Asp145, while the phenyl and allyl moieties establish van der Waals carbon–carbon interactions (3.2 Å < d < 3.8 Å) with neighboring residues. Compounds with aminothiazole hinge-binding scaffolds have been previously described as inhibitors of checkpoint kinase I,[24] p38α/MAPK,[25] CDK2,[26] and CDK5.[27−29] However, the diaminothiazole CDK-inhibitors developed herein are unique with respect to structure, potency, and selectivity.

Structure–Activity Relationship (SAR) Studies. Analogues of **1** were designed such that the hinge-binding functionality of the aminothiazole core remained unchanged, while the flanking allyl (R1) and phenyl (R2) moieties were systematically modified (Figure 2, Table 1). A total of 95 analogues were synthesized and evaluated using three different enzymatic assays based on their inhibitory activities (see Experimental Section). The pyruvate kinase/lactate dehydrogenase (PK–LDH) spectrophotometric assay was employed for HTS and initial SAR studies. As the CDK2–cyclin A concentration in the PK–LDH assay limits the determination of IC_{50} values up to ~0.1 μM, a more sensitive fluorescence-based assay was employed for inhibitors with submicromolar activities, which allowed accurate IC_{50} determinations up to ~0.02 μM (Figure S1 of Supporting Information). Activities of the most potent compounds were determined using a highly sensitive P^{33}-radiolabeled activity assay.[30] The pan-kinase inhibitor staurosporine (IC_{50} < 1 nM against CDK2–cyclin A) served as a control. Crystal structures of 35 CDK2–inhibitor complexes were determined between 1.4 and 2.0 Å resolution (Table S1 of Supporting Information). Scheme 1 shows the general method for synthesis of the targeted compounds. An isothiocyanate is reacted with cyanamide in the presence of *tert*-butoxide in THF for 15 min to form the intermediate addition product, which is directly reacted with a bromoacetyl derivative to form the desired (2,4-diaminothiazol-5-yl)methanone derivative.

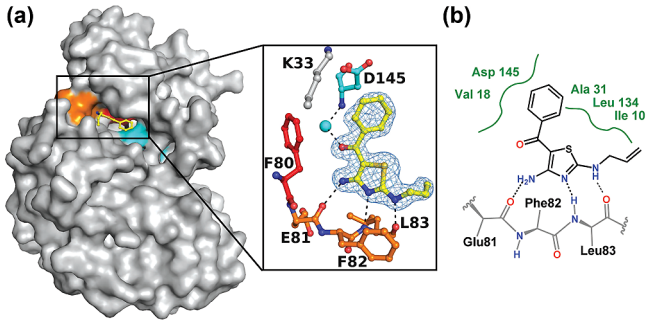

Figure 1. Interaction of HTS hit compound **1** with CDK2. (a) The cocrystal structure of CDK2 with hit **1** revealed a typical type I mechanism of action by binding through the hinge-region of the ATP site. The enzyme is shown in gray, with the hinge region (residues 81–83) highlighted in orange, gatekeeper residue Phe80 in red, and DFG motif in cyan. The exploded view shows the hydrogen bonding interactions between the inhibitor (yellow) and enzyme residues including Asp145 of the DFG motif. Water molecules are shown as cyan spheres. The $2F_o - F_c$ electron density map at 1.85 Å resolution is shown as blue mesh, contoured at 1σ around the inhibitor. The $F_o - F_c$ omit map is shown in the Supporting Information (Figure S5). (b) Schematic representation of hydrogen bonding (dotted lines) and hydrophobic interactions (green). PDB: 3QQK.

Modifications to R2 resulted in analogues **2–15** (Table 1a), of which the *meta*-pyridine analogue (**3**) was 5-fold more active (IC_{50} = 3.1 μM) than the parent compound. This is likely due to the weak hydrogen bonding potential of the pyridine nitrogen with the ε-amino group of Lys33 (Figure 3a), which establishes a salt bridge with Glu51 of the PSTAIRE helix in the activated CDK2–cyclin A2 complex.[31] Remarkably, substitution with *ortho*- or *para*-pyridine (**6**, **10**) resulted in loss of activity, and cocrystal structures suggest that Lys33 is no longer attracted to the pyridine ring (Figure 3b, 3c). Moreover, binding of **10** induced a large conformational change in the P-loop (residues Gly11–Val18), allowing a water molecule to enter and to interact with the ring nitrogen, while **6** adopts an unfavorable conformation upon binding to the active site. Modifications to R1 yielded analogues **16–25** (Table 1b), of which the phenyl (**16**) and cyclohexyl (**17**) substituents yielded more than a 15-fold improvement in activity over the parent compound. Combination of a *meta*-pyridine ring at R2 (as in compound **3**) with a phenyl group at R1 (as in compound **16**) further improved inhibitory activity (**30**, IC_{50} = 0.65 μM). However, with a phenyl group at R1, substituents at R2 other than *meta*-pyridine were not tolerated as well or were detrimental to compound activity (Table 1c). Bulky R1

dx.doi.org/10.1021/jm301234k | J. Med. Chem. 2013, 56, 3768–3782

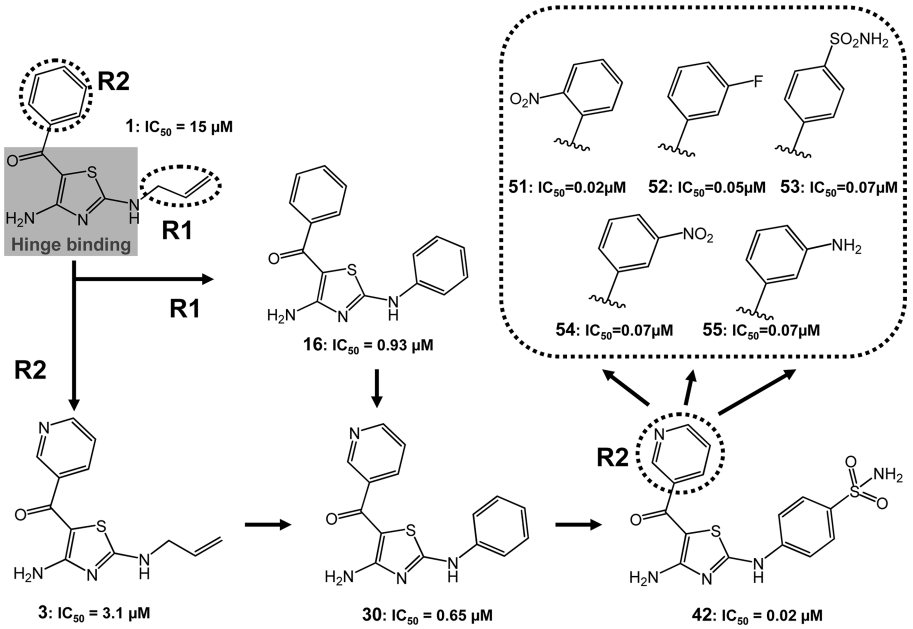

Figure 2. SAR milestones in the optimization of hit compound **1**.

functional groups extend into a region commonly referred to as the front specificity pocket, consisting of residues Gln85, Asp86, and Lys89. To interrogate this pocket, we next synthesized a series of analogues with *meta*-pyridine at R2 and diverse substituents at R1 (Table 1d). Introduction of a sulfonamide moiety at the *para* position of the phenyl ring yielded significant improvement over the parent compound (**42**, IC_{50}= 0.02 μM). Using the fluorescence-based assay, the CDK2−cyclin A concentration of 9 nM became limiting for highly potent inhibitors such as **42**. Even the pan-kinase inhibitor staurosporine, which is a known subnanomolar inhibitor of CDK2−cyclin A, displayed an IC_{50} value of 20 nM in the fluorescence-based assay. Therefore, a highly sensitive P^{33}-radiolabel assay was employed, in which **42** inhibited the CDK2−cyclin A complex with an IC_{50} value of 0.9 nM (Figure S2 of Supporting Information), rendering this compound among the most potent CDK2 inhibitors reported to date.[17] This 15000-fold increase in activity over the parent compound is primarily attributed to an elaborate hydrogen bonding network between the sulfonamide group and residues His84, Gln85, Asp86, and Lys89 (Figure 4a). Of the other R1 substituents tested, the *para*-benzamide also conferred a considerable increase in activity (**43**, IC_{50}= 0.22 μM). Introduction of a sulfonamide group in the *meta* position resulted in a loss of activity (**49**, IC_{50} = 7.8 μM), and modifications to **49** did not restore inhibitory activity (**78**−**83**, Table S2 of Supporting Information).

Several analogues of **42** were prepared with modifications to R2, of which compounds **51**−**55** were the most potent inhibitors, with IC_{50} values between 0.02 and 0.07 μM (Table 1e). Using the P^{33}-radiolabeled assay, **51** inhibited CDK2−cyclin A2 with an IC_{50} value of 1.5 nM (Figure S2 of Supporting Information). Intriguingly, the *ortho*-nitro group of **51** is nested in a hydrophobic pocket composed of residues Val18, Ala31, Lys33, and gatekeeper Phe80 (Figure 4b). The unusual proximity and orientation of the nitro group toward the Phe80 side chain indicate attractive interactions through van der Waals forces or the establishment of "nonclassical" hydrogen bonds between the phenyl ring and the nitro group, a phenomenon previously described for the interaction of nitro-substituted inhibitors of aldolase reductase with an active site tyrosine ring.[32] This notion is supported by the observation that other substitutions in the *ortho* position, such as methyl (**62**) or methylester (**68**), were detrimental to inhibitory activity. Although **52**−**55** displayed similar activities, the binding interactions of the respective R2 substituents are markedly different (Figure 5). The *meta*-substituents of **52** (fluorine), **54** (nitro), and **56** (methoxy) share the same binding pocket, composed of residues Gly13, Val18, Lys33, and Asp145, whereas the *meta*-amino group of **55** causes the ring to rotate by ∼180° to form hydrogen bonds with Gln131 and Asn132. Other *meta*-substituents, such as trifluoromethyl (**58**), hydroxy (**59**), or chlorine (**65**), significantly decreased inhibitory activity. The *para*-sulfonamide moiety of **53** establishes hydrogen bonding interactions with Asn 132 and Asp145, but other *para* substituents, such as nitro (**63**), amino (**64**), methoxy (**65**), or bulky functional groups, resulted in loss of activity. Combined, these findings indicate that anchoring the inhibitor through a sulfonamide moiety in R1 allows diverse R2 substituents to efficiently interact with residues around Asp145 and the P-loop. Notably, introduction of aniline substituents in R1 to mimic the triazole carbothioamide structure of the highly potent pan-kinase inhibitor CDK1/2 inhibitor III resulted in complete loss of activity (Table S6 of Supporting Information).

Kinase Profiling. To assess kinase selectivity, a representative set of inhibitors was initially profiled against a panel of 48 different kinases (Figure S3 of Supporting Information). GSK3β, a well-known cross-reactive target of CDK2 inhibitors,[33,34] was the only other kinase significantly affected by these compounds. Next, compound **51** was thoroughly characterized using the P^{33}-radiolabeled assay against a panel of different CDK−cyclin complexes together with GSK3β (Table 2, Figure S4 of Supporting Information). The highest inhibitory activity was seen against CDK2 and CDK5 (IC_{50} values between 1.1 and 1.8 nM), followed by CDK1, CDK4, and CDK6 (IC_{50} values between 4.0 and 7.6 nM), CDK9 and CDK3 (IC_{50} values of 13 and 38 nM), and CDK7 (IC_{50} > 1

dx.doi.org/10.1021/jm301234k | J. Med. Chem. 2013, 56, 3768−3782

Table 1. CDK2−Cyclin A2 Inhibitory Activities of Analogues of Hit Compound 1[b]

(a)

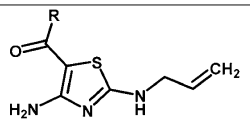

1 - 15

R				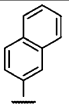			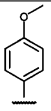	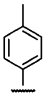
Compound	**1**	**2**	**3**	**4**	**5**	**6**	**7**	**8**
IC_{50} (μM)	15	2.9	3.1	5	12	33	35	37
PDB ID	3QQK	3R8V	3QTQ	3R8U	3S00	3S0O	-	-

R	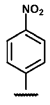					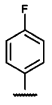	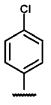
Compound	**9**	**10**	**11**	**12**	**13**	**14**	**15**
IC_{50} (μM)	41	49	>100	>100	>100	>100	>100
PDB ID	-	3R8Z	-	-	-	-	-

(b)

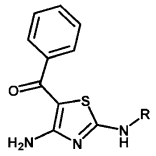

16 - 25

R										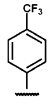
Compound	**16**	**17**	**18**	**19**	**20**	**21**	**22**	**23**	**24**	**25**
IC_{50} (μM)	0.93	1.3	2.0	5.7	8.9	15	17	95	>100	>100
PDB ID	3QTR	-	-	3RJC	-	-	-	-	-	-

(c)

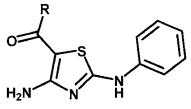

30 - 41

R		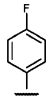				
Compound	**30**	**31**	**32**	**33**	**34**	**35**
IC_{50} (μM)	0.65	1.4	1.6	2.2	3.1	99
PDB ID	3QTW	-	-	-	3QTS	-

R	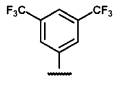				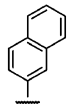	
Compound	**36**	**37**	**38**	**39**	**40**	**41**
IC_{50} (μM)	>100	>100	>100	>100	>100	>100
PDB ID	-	3RPR	-	-	-	3RZB

dx.doi.org/10.1021/jm301234k | J. Med. Chem. 2013, 56, 3768−3782

Table 1. continued

(d)

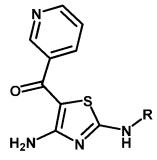

42 - 50

R	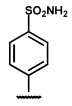	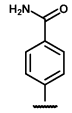			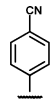	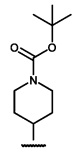	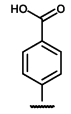	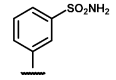	
Compound	**42**	**43**	**44**	**45**	**46**	**47**	**48**	**49**	**50**
IC_{50} (μM)	0.02 (0.0009)[a]	0.2	0.52	0.38	2.8	3.5	4.0	7.8	43
PDB ID	3QU0	3RK7	3RK9	3RKB	-	-	3RK5	-	-

(e)

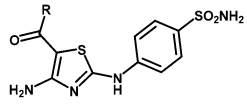

51 - 71

R							
Compound	**51**	**52**	**53**	**54**	**55**	**56**	**57**
IC_{50} (μM)	0.02 (0.0015)[a]	0.05	0.07	0.07	0.07	0.1	0.13
PDB ID	3QXP	3QTZ	3QTU	3QTX	3RPV	3RAL	3RAK

R							
Compound	**58**	**59**	**60**	**61**	**62**	**63**	**64**
IC_{50} (μM)	0.57	1.5	3.5	4.8	4.8	7.4	8.8
PDB ID	-	-	-	3RPY	3SQQ	-	-

R		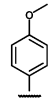	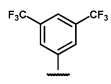		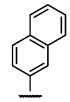	
Compound	**65**	**66**	**67**	**68**	**69**	**71**
IC_{50} (μM)	15	17	25	32	82	>100
PDB ID	-	3S1H	-	-	3RMF	-

[a]Value determined by P^{33}-radiolabeled assay. [b]Values represent the mean of duplicate or triplicate dose−response measurements with a standard deviation of <10%.

μM). Notably, **51** was 90-fold less active against GSK3β. Comparison of **51** and staurosporine showed similar activities against most of the enzymes tested, with the exception of CDK1, CDK3, and GSK3β, which were significantly more tolerant toward **51**. Finally, compound **51** was tested against a panel of 339 kinases by Reaction Biology Corporation at a

dx.doi.org/10.1021/jm301234k | J. Med. Chem. 2013, 56, 3768−3782

Scheme 1

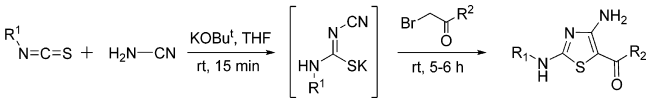

single concentration of 0.1 μM ($\approx 100 \times IC_{50}$) (Figure 6, Table S7 of Supporting Information). The data confirmed that **51** is highly selective against CDKs within the human kinome (Figure 6b). Compound **51** displayed highest inhibitory activity against CDK5 and CDK2 (95−96%), followed by CDK9 and CDK1 (90−93%) and CDK4 and CDK6 (87 and 85%). GSK3α and ERK7 were inhibited to 73−75%, followed by TAO1, GSK3β, and CLK2 (60−66%). The vast majority of kinases (282) were not affected by compound **51**.

Cellular Activity. Compounds with the highest activity against the CDK2−cyclin A complex were evaluated for inhibitory potential against a total of 15 cancer cell lines and three testis cell lines. Initial studies were performed on the proliferation/survival of MDA-MB-468 breast cancer cells treated with increasing concentrations of inhibitors for 72 h and determined by MTT assay. Compound **51** significantly inhibited cell viability in a concentration-dependent manner with an IC_{50} value of 0.3 μM (Table 3, Figure S6 of Supporting Information). In contrast, **42** was much less potent (IC_{50} = 2.8 μM), suggesting that the R2 pyridine moiety negatively impacts cellular uptake of the inhibitor. This is supported by the observation that the pyridine-containing **45** was equally less effective (IC_{50} = 3.1 μM) as compared to **51**, whereas the fluorophenyl moiety of **52** conferred higher cellular activity (IC_{50} = 0.85 μM). As expected from its poor in vitro activity against CDK2, compound **69** displayed the lowest ability to inhibit MDA-MB-468 cells (IC_{50} = 5.5 μM). To assess the ability of the compounds to selectively inhibit the division of testis cells important for spermatogenesis, MTT assays were carried out using cell lines that represent important spermatogenic stages where cell division is critical for maintenance of spermatogenesis: spermatogonia (GC-1)[35,36] and spermatocytes (GC-2).[36,37] The results were compared to TM-4 cells,[38,39] which represent Sertoli cells that normally stop dividing by the time spermatogenesis has commenced. Most compounds showed moderate to poor activity against these cell lines, with IC_{50} values between 4 and 20 μM (Table 3). Compounds **51**, **52**, and **57** showed higher activity against spermatocyte-derived cells (GC2) over spermatogonial-derived cells (GC1) cells and a Sertoli cell line (TM-4).

Next we determined the cellular activity of compounds **51**, **52**, **53**, **55**, and **69** against a panel of 14 different cancer cell lines using a resazurin/resorufin-based fluorescence assay (Table 4). The potent cell active CDK2 inhibitor dinaciclib and the antineoplastic drug doxorubicin served as positive controls. Compound **51** inhibited the proliferation/survival of four cell lines (A-673, SK-Br-3, SK-ES-1, and T-47D) with IC_{50} values between 0.27 and 0.56 μM, eight cell lines (SK-UT-1, MDA-MB-231, H929, U266, MDA-MB-436, MNNG HOS, MCF-7, and SW-872) were moderately inhibited with IC_{50} values between 1.4 and 6.9 μM, and two cell lines (RPMI-8226 and BT-549) were largely tolerant with IC_{50} values >10 μM. Compound **52** displayed a similar activity profile with IC_{50} values between 0.45 and 6.8 μM for 13 cell lines but was significantly less active in those cell lines that were prominently inhibited by **51**. The weak CDK2 inhibitor **69** was largely ineffective, and the potent CDK2 inhibitors **53** and **55** were also ineffective, presumably due to poor cell permeability. As expected, dinaciclib was extremely effective against most cell lines with IC_{50} values between <0.005 and 0.01 μM. Notably, the BT-549 cell line was tolerant to all CDK2 inhibitors including dinaciclib but was sensitive to doxorubicin (IC_{50} = 0.11 μM).

Mechanism of Action of Compound 51. To evaluate if the antiproliferative activity of **51** is caused by inhibition of cellular CDK2, we selected inhibition of Rb phosphorylation at the CDK-specific sites Ser807/811 and activation of caspase-3 at the onset of apoptosis as mechanism-based markers for CDK-specific inhibitors.[8,22] The most sensitive cell line (A-673) and a moderately inhibited H929 cell line were treated for 24 h with compound **51** or dinaciclib and were evaluated by immunoblotting and caspase-3 activation (Figure 7). Compound **51** suppressed phosphorylation of the Rb protein above 0.25 μM in A-673 cells (Figure 7a), which is in accord with the IC_{50} value of 0.27 μM in cell viability assays. The activity of caspase-3 was increased by 196% with a half-maximal effective concentration (EC_{50}) of 0.4 μM. Dinaciclib completely suppressed phosphorylation of Rb Ser807/811 at 0.05 μM

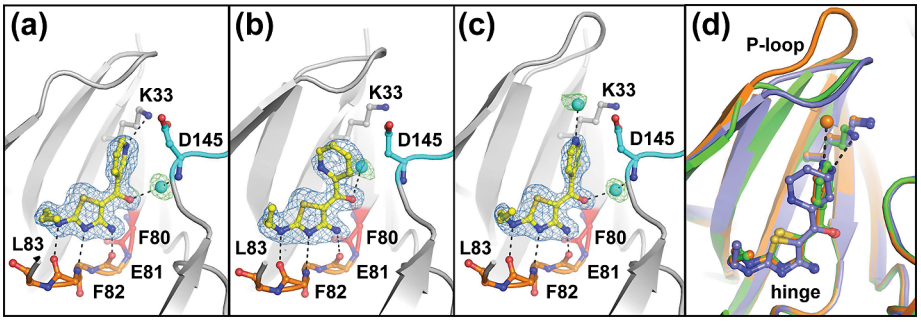

Figure 3. Influence of R2 pyridine substituents on binding interactions with CDK2. Crystal structures of CDK2 liganded with the pyridine analogues **3** (a), **6** (b), and **10** (c). *meta*-Pyridine (**3**) attracts the ϵ-amino group of Lys33, whereas *para*-pyridine (**10**) induces a large conformational change in the P-loop, allowing a water molecule to interact with the ring nitrogen. The *ortho*-pyridine (**6**) adopts a conformation unfavorable for interaction with CDK2. Figure 3d shows the differences in binding interactions upon superposition of the crystal structures. The enzymes are shown in gray with the hinge region (residues 81−83) colored in orange, the gatekeeper Phe80 residue in red, and Asp145 of the DFG motif in cyan. The hydrogen bonding interactions between the inhibitors (yellow) and enzyme residues are shown as black dotted lines. The key water molecules are shown as cyan spheres, with the $2F_o - F_c$ electron density map shown as a blue mesh around the inhibitor, and a green mesh around the water both contoured at 1σ. PDB entries 3QTQ, 3S0O, and 3R8Z.

dx.doi.org/10.1021/jm301234k | J. Med. Chem. 2013, 56, 3768−3782

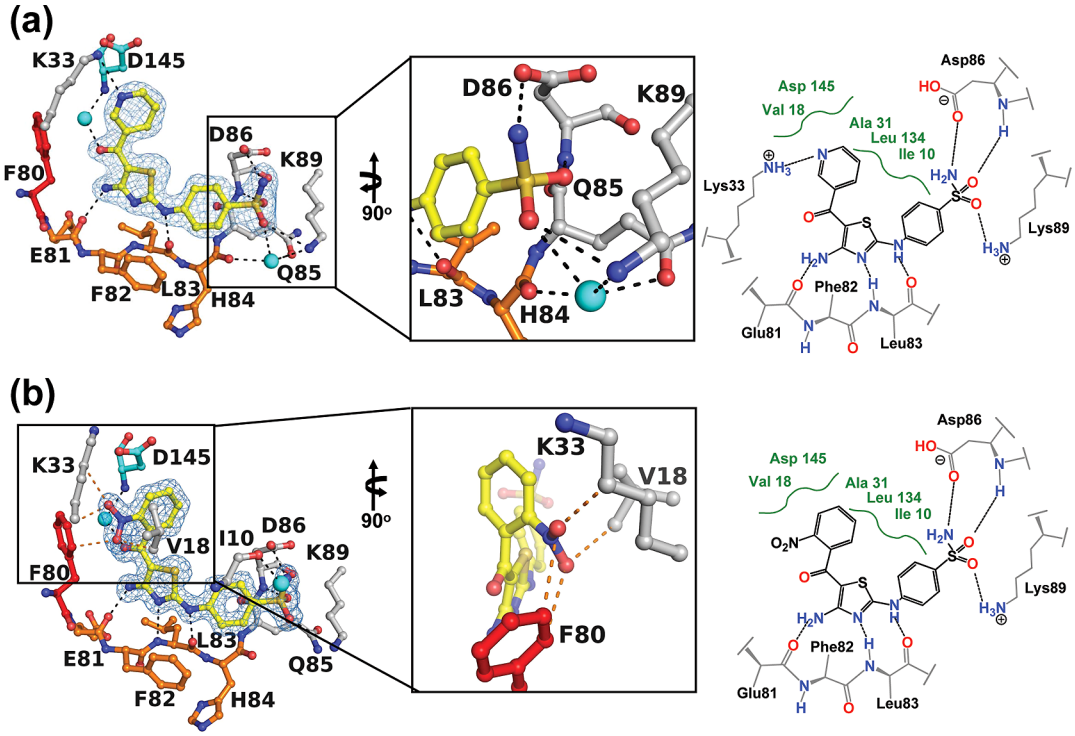

Figure 4. Interaction of sulfonamide analogues **42** and **51** with CDK2. Crystal structures of the most potent inhibitors **42** (a) and **51** (b). Addition of a *para*-phenyl sulfonamide moiety at R1 substantially increased the inhibitory activity through establishment of a hydrogen bonding network with residues of the front specificity pocket (top exploded view). Addition of an *ortho*-nitrophenyl group at R1 of **51** retained the high in vitro activity and substantially increased cellular activity. The exploded view (bottom) shows the unusual proximity of the nitro group to neighboring hydrophobic residues. The $2F_o - F_c$ electron density is displayed as blue mesh, contoured at 1σ around the compound. Hydrogen bonding and potential π-bonding interactions are shown as black and orange dotted lines, respectively. $F_o - F_c$ electron density maps from refinements omitting the inhibitors are shown in the Supporting Information (Figure S5). Schematic representations of the respective CDK2−inhibitor interactions are shown in the right panel. Black dotted lines indicate hydrogen bonding interactions, while van der Waals (hydrophobic) interactions are shown in green. PDB entries 3QU0 and 3QXP.

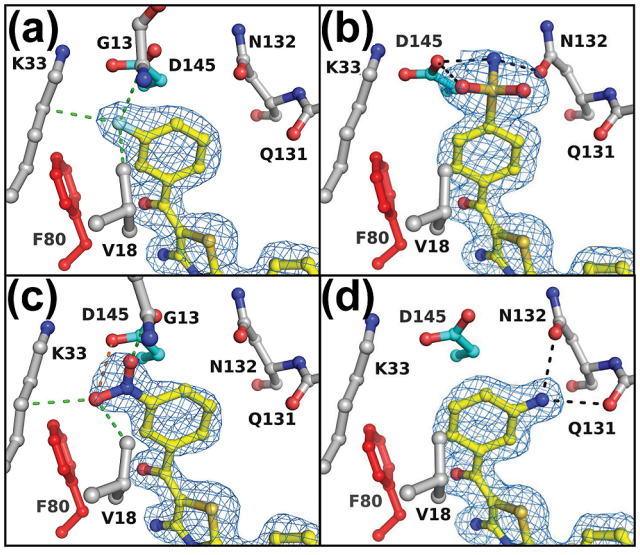

Figure 5. Sulfonamide inhibitors tolerate diverse R2 substituents. Crystal structures of CDK2 liganded with **52** (a), **53** (b), **54** (c), and **55** (d), other highly potent inhibitors of the *para*-sulfonamide series of Table 1e. The respective $2F_o - F_c$ density maps, contoured at 1σ, are shown as blue mesh. Black, green, and orange dotted lines indicate potential hydrogen bonding, hydrophobic, and π-interactions, respectively. PDB entries 3QTZ, 3QTU, 3QTX, and 3RPV.

Table 2. Inhibitory Activity of Compound 51 against Various CDK−Cyclin Complexes and GSK3β Using the P^{33}-Radiolabeled Assay

kinase	compound **51** IC_{50} (nM)	staurosporine IC_{50} (nM)
CDK1/cyclin A	7.6 ± 0.7	1.7 ± 0.1
CDK2/cyclin A	1.1 ± 0.1	0.4 ± 0.03
CDK2/Cyclin A1	1.8 ± 0.2	0.5 ± 0.04
CDK3/cyclin E	38 ± 5.3	4.0 ± 0.6
CDK4/cyclin D1	4.0 ± 0.2	6.6 ± 0.2
CDK5/p25	1.5 ± 0.2	1.2 ± 0.1
CDK6/cyclin D1	6.6 ± 0.3	2.9 ± 0.1
CDK7/cyclin H	>1000	910 ± 115
CDK9/cyclin K	13 ± 1.0	13 ± 0.5
GSK3b	107 ± 20	15 ± 1.1

and increased caspase-3 activity by 280% with an EC_{50} value of 0.011 μM. Similar results were obtained for H929 cells (Figure 7b), which displayed inhibition of Rb phosphorylation above 1.5 μM (IC_{50} = 1.8 μM in viability assays). Upon treatment with 1.5 μM of compound **51**, 26−59% of the cells were apoptotic. Dinaciclib suppressed the phosphorylation of Rb at 0.005 μM with 63−84% apoptotic cells. The correlation between the suppression of Rb-phosphorylation and onset of apoptosis suggests that the mechanism of action of compound **51** in these two cancer cell lines may proceed through inhibition of CDKs critical for the phosphorylation of Rb protein at Ser807/811.

dx.doi.org/10.1021/jm301234k | J. Med. Chem. 2013, 56, 3768−3782

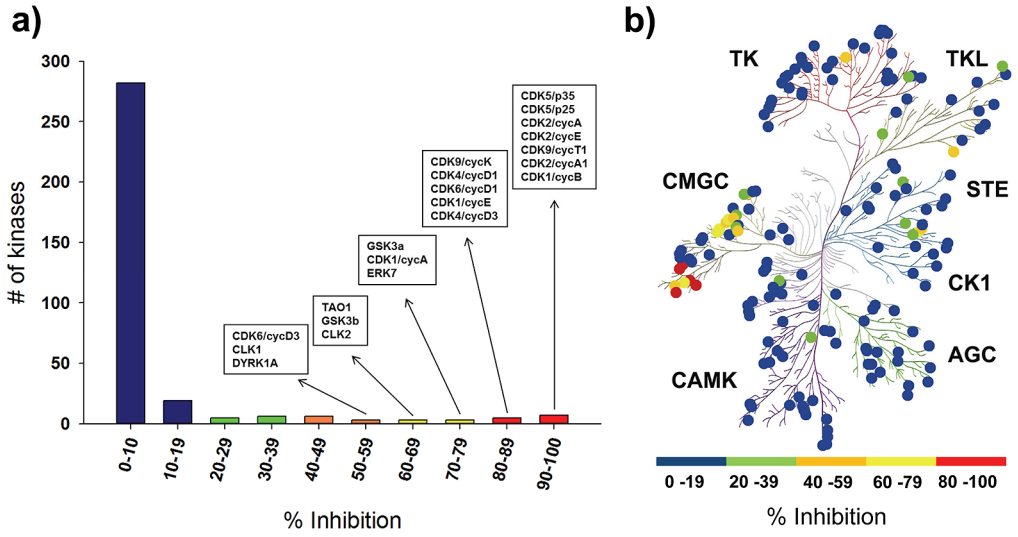

Figure 6. Profiling of compound **51** against a panel of 339 kinases. (a) Quantitative distribution of kinases binned according to the inhibition by compound **51**. (b) Distribution of inhibited kinases within the human kinome. The color code for inhibition is indicated. Residual enzymatic activity was determined in single dose duplicate at a compound concentration of 0.1 μM. The ATP concentration was 10 μM. Staurosporine served as a positive control. The experiment was performed by Reaction Biology Corp. using a P^{33}-radiolabel assay. The data sets are shown in Table S7 of Supporting Information.

Table 3. Cellular Activity of Inhibitors against MDA-MB-468 Breast Cancer and Testis Cell Lines As Determined by MTT Assay

	cell line			
compd	MDA-MB-468 IC_{50} (μM)[a]	TM-4 IC_{50} (μM)[a]	GC-2 IC_{50} (μM)[a]	GC-1 IC_{50} (μM)[a]
16	nd	12 ± 1.1	11 ± 1.0	11 ± 1.0
17	nd	9.3 ± 1.0	8.2 ± 1.0	9.2 ± 1.1
30	nd	5.5 ± 1.1	9.5 ± 1.1	5.9 ± 1.0
31	nd	14 ± 1.1	17 ± 1.1	16 ± 1.0
32	nd	5.1 ± 1.0	4.1 ± 1.1	3.6 ± 1.0
41	nd	>60	>60	>60
42	2.8 ± 0.3	13 ± 4.9	>30	20 ± 1.7
45	3.1 ± 0.2	nd	nd	nd
51	0.3 ± 0.1	16 ± 1.1	9.0 ± 1.2	20 ± 1.7
52	0.8 ± 0.1	4.8 ± 1.0	3.9 ± 1.0	6.4 ± 1.1
54	nd	4.0 ± 0.6	20 ± 5.4	22 ± 6.7
56	nd	6.4 ± 1.5	11 ± 1.2	9.1 ± 1.1
57	nd	9.1 ± 1.1	6.1 ± 1.0	17 ± 1.1
69	5.5 ± 0.5	nd	nd	nd

[a]Average of dose–response experiments performed in triplicate using 9 inhibitor concentrations between 0.02 and 100 μM (nd = not determined).

CONCLUSIONS

Starting from a single HTS hit compound with weak inhibitory activity, we employed protein crystallography as the main tool to design novel, highly potent, and selective inhibitors of CDK2 as potential leads for further development as chemical probes or therapeutics. Throughout the course of this project, 35 high-resolution cocrystal structures of CDK2 were determined for distinct analogues of the hit compound, with inhibitory activities ranging from excellent (IC_{50} = 0.001 μM) to poor (IC_{50} > 25 μM). The comprehensiveness of crystallographic structure–activity relationship data for a single chemical scaffold against a single target protein is unprecedented to our knowledge and may provide valuable guidance for the refinement of algorithms used in molecular docking simulations and structure-based drug design.

Extensive kinase profiling indicates that compound **51** is highly selective for CDKs, with preference for CDK2 and CDK5 over CDK9, CDK1, CDK4, and CDK6. Among the inhibitors tested, only compound **51** significantly inhibited the proliferation/survival of cancer cells with IC_{50} values ≤0.5 μM in five of the 15 cancer cell lines tested. Mechanism-based marker analysis established that the cellular activity of **51** correlates with the suppression of Rb-phosphorylation and the onset of apoptosis. The observation that the reportedly Rb-deficient cell line BT-549[40] is insensitive to compound **51** and dinaciclib (Table 4) seems to corroborate the notion that suppression of Rb-phosphorylation is the primary mode of action of **51**. However, the MDA-MB-468 cell line is also Rb-deficient but sensitive to **51** (Table 3), indicating the involvement of other essential CDK substrates or possible off-target interactions. A more thorough cell-based study is planned to further address the mechanism of action of this inhibitor series using multiple marker analysis.[8] Although compound **51** and dinaciclib share similar CDK inhibitory and selectivity profiles in enzymatic activity assays, dinaciclib is an extremely potent antiproliferative compound in cancer cell lines.[8,22] The modest activity of our inhibitors in cell-based assays suggests poor cell permeability, and a new series of compounds is planned with suitable solubilizing groups in solvent exposed regions to facilitate cellular uptake. Combined, these results demonstrate the potential of these inhibitors for further development into CDK-specific chemical probes and therapeutics.

EXPERIMENTAL SECTION

Reagents and Compounds. Reagents and compounds for biochemical and crystallization experiments were purchased from Sigma-Aldrich (St. Louis, MO) and Hampton Research (Aliso Viejo, CA) unless otherwise indicated. Compounds **1**, **5**, **8**, **11**–**14**, and **19** were purchased from Sigma-Aldrich, Ryan Scientific (Mt. Pleasant, SC), ChemDiv (San Diego, CA), and Labotest OHG (Niederschoena, Germany). Staurosporine was purchased from Tocris Bioscience

dx.doi.org/10.1021/jm301234k | J. Med. Chem. 2013, 56, 3768–3782

Table 4. Cellular Activity of Inhibitors against a Panel of 14 Cancer Cell Lines As Determined by a Resazurin/Resorufin-Based Fluorescent Viability Assay

	compd						
cell line	**51** IC_{50} (μM)[a]	**52** IC_{50} (μM)[a]	**53** IC_{50} (μM)[a]	**55** IC_{50} (μM)[a]	**69** IC_{50} (μM)[a]	dinaciclib IC_{50} (μM)[a]	doxorubicin IC_{50} (μM)[a]
A-673 rhabdomyosarcoma	0.27	0.45	>10	8.8	3.7	<0.005	0.17
SK-Br-3 adenocarcinoma	0.49	1.2	>10	4.1	6.1	<0.005	0.09
SK-ES-1 osteosarcoma	0.56	1.1	>10	9.8	4.8	<0.005	0.042
T-47D ductal carcinoma	0.5	0.98	8.7	5.8	4.5	0.01	0.1
SK-UT-1 leiomyosarcoma	1.4	1.6	>10	>10	10	0.006	0.076
MDA-MB-231 adenocarcinoma	1.5	1.2	>10	>10	>10	<0.005	0.17
H929 myeloma	1.6	1	>10	6.8	4.3	<0.005	0.065
U266 myeloma	1.8	1.5	7.2	5.5	7.9	0.006	0.67
MDA-MB-436 adenocarcinoma	2	1.3	>10	>10	5.3	<0.005	0.1
MNNG HOS osteosarcoma	3	2.2	>10	>10	9.7	0.0055	0.59
MCF-7 adenocarcinoma	3.1	1.3	>10	>10	5.9	0.02	0.24
SW-872 liposarcoma	6.9	3.1	>10	>10	>10	0.0095	0.14
RPMI-8226 myeloma	>10	6.8	>10	>10	>10	0.009	0.27
BT-549 ductal carcinoma	>10	>10	>10	>10	>10	>10	0.11

[a]Average of three data sets, each consisting of dose−response experiments performed in quadruplicate using nine inhibitor concentrations between 0.004 μM and 12.5 μM.

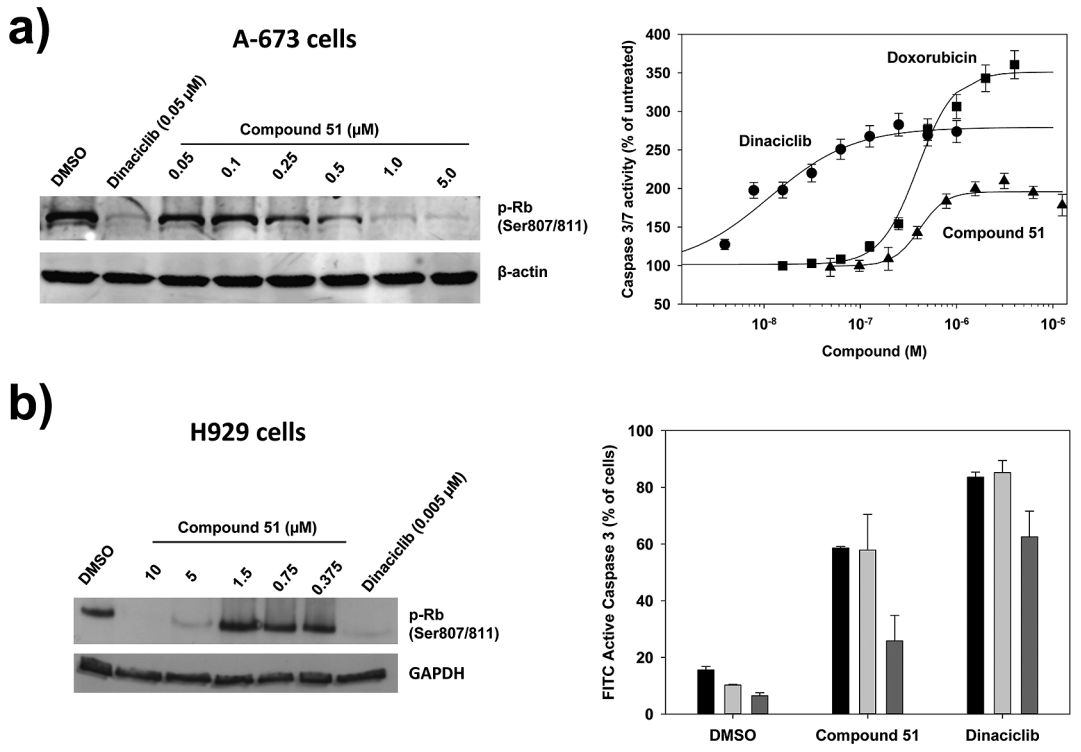

Figure 7. Mechanism of action of compound **51**. (a) Asynchronously growing A-673 sarcoma cells were treated with increasing concentrations of compound **51** for 24 h, and cell lysates were analyzed for phosphorylation of Rb protein at Ser807/811 by immunoblotting (left). Dinaciclib (0.05 μM) served as a positive inhibitor control and actin as a loading control. Onset of apoptosis was assessed by measuring the activity of caspase 3 using a bioluminescent assay upon 24 h treatment of cells with increasing concentrations of compound 51 (▲), dinaciclib (●), or doxorubicin (■) (right). Dinaciclib and doxorubicin served as positive controls. The EC_{50} values for caspase-3 activation were 0.41 μM for compound **51**, 0.011 μM for dinaciclib, and 0.39 μM for doxorubicin, which served as a positive control for the onset of apotosis. (b) Asynchronously growing H929 myeloma cells were treated for 24 h with compound **51** or dinaciclib and phosphorylation of Rb protein was analyzed by immunoblotting (left). Onset of apoptosis was assessed by measuring the level of cleaved, activated caspase 3 using flow cytometry (right). Shown are the percentages of cells with increased caspase-3 levels upon treatment with 1.5 μM compound **51** or 0.005 μM dinaciclib from three experiments.

(Minneapolis, MN). The peptide substrate for activity assays was synthesized by Biomatik (Wilmington, DE). Protein concentrations were determined by the Bradford method using Bio-Rad protein assay reagent (Bio-Rad, Hercules, CA), with bovine serum albumin as a standard. The concentration of crystallization-grade proteins was determined by A_{280} molar absorbance using a nanodrop ND-1000 spectrophotometer (Nanodrop Technologies, Wilmington, DE). Nonlinear regression analysis was performed using SigmaPlot (Systat Software, Chicago, IL). Cloning, expression, and purification of CDK2, cyclin A2, and CAK1 were performed as described previously.[41]

dx.doi.org/10.1021/jm301234k | J. Med. Chem. 2013, 56, 3768−3782

DMEM, penicillin, and streptomycin were purchased from Invitrogen (Carlsbad, CA). Fetal bovine serum was obtained from Atlanta Biologicals (Atlanta, GA), and MTT reagent was purchased from Sigma-Aldrich.

Chemical Synthesis. Commercially available chemicals were used as purchased without further purification. THF was dried over an activated alumina column before use. ^{1}H NMR spectra were obtained on a 400 MHz spectrometer, and chemical shifts (ppm) were referenced to the residual solvent peak. ^{13}C NMR spectra were recorded at 100 MHz, and chemical shifts (ppm) were referenced to the appropriate residual solvent peak. High-resolution mass spectra (HRMS) were recorded with electrospray ionization. NMR spectra are shown in the Supporting Information. Compounds were purified by HPLC to >95% purity as reflected by their ability to readily cocrystallize with CDK2. The synthesis of **42** is given as a representative procedure that was used for the synthesis of the targeted library (* denotes that cocrystal structures with CDK2 were obtained).

*4-(4-Amino-5-nicotinoylthiazol-2-ylamino)benzenesulfonamide (**42**). At 20 °C, a mixture of 4-isothiocyanatobenzenesulfonamide (2.14 g, 10 mmol) and cyanamide (0.42 g, 10 mmol) in tetrahydrofuran (35 mL) was treated with potassium *tert*-butoxide (2.46 g, 22 mmol) for 15 min. 3-(2-Bromoacetyl)pyridinium bromide (2.66 g, 9.5 mmol) was added, and the suspension was stirred for 6 h. The solvent was removed, and the semisolid residue was triturated with water to give the crude product, which was filtered and dried in a vacuum oven at 50 °C for 2 h. The dried crude product was recrystallized from EtOAc:DMF (8:2), which provided 2.2 g (60%) of 4-(4-amino-5-nicotinoylthiazol-2-ylamino)benzenesulfonamide as a yellow solid: mp (EtOAc/DMF) 218−220 °C. ^{1}H NMR (400 MHz, DMSO-d_6) δ 11.18 (s, 1H), 8.86 (d, J = 1.7 Hz, 1H), 8.69 (dd, J = 4.8, 1.6 Hz, 1H), 8.33 (s, 2H), 8.13−7.97 (m, 1H), 7.85−7.72 (m, 4H), 7.52 (ddd, J = 7.9, 4.8, 0.6 Hz, 1H), 7.29 (s, 2H). ^{13}C NMR (100 MHz, DMSO-d_6) δ 180.6, 166.6, 165.5, 151.3, 147.6, 142.3, 138.2, 137.1, 134.5, 127.0, 123.7, 118.3; HRMS calcd for $C_{15}H_{14}N_5O_3S_2$ (M + H) 376.0538, found 376.0549.

Physical Chemical Properties. Solubility: 1.4 μM. Plasma protein binding: 84%. In vitro absorption (Caco-2, ph 6.5/7.4): A−B = 1.0 × 10^{-6}; B−A = 24.5 × 10−6.

*(2-(Allylamino)-4-aminothiazol-5-yl)(3-nitrophenyl)methanone (**2**).* Brown solid: mp (EtOAc/MeOH) 167−169 °C. ^{1}H NMR (400 MHz, DMSO-d_6) δ 8.89 (s, 1H), 8.80 (d, J = 1.5 Hz, 1H), 8.63 (dd, J = 4.7, 1.3 Hz, 1H), 8.55−7.61 (m, 3H), 7.46 (ddd, J = 7.9, 4.8, 0.6 Hz, 1H), 5.86 (ddd, J = 22.2, 10.3, 5.1 Hz, 1H), 5.24 −5.04 (m, 2H), 3.91 (s, 2H). ^{13}C NMR (100 MHz, DMSO-d_6) δ 178.2, 167.2, 147.6, 143.2, 133.7, 133.1, 130.2, 124.7, 121.4, 116.4, 46.1. HRMS calcd for $C_{13}H_{13}N_4O_3$ S (M + H) 305.0708, found 305.0694.

*(2-(Allylamino)-4-aminothiazol-5-yl)(pyridin-3-yl)methanone (**3**).* Yellow solid: mp (EtOAc/hexane) 184−186 °C. ^{1}H NMR (400 MHz, DMSO-d_6) δ 8.94 (s, 1H), 8.35−8.65 (m, 2H), 8.30 (dd, J = 8.1, 2.0 Hz, 1H), 8.07 (d, J = 7.7 Hz, 2H), 7.75 (t, J = 7.9 Hz, 1H), 5.87 (ddd, J = 22.0, 10.2, 5.1 Hz, 1H), 5.18 (ddd, J = 13.7, 11.6, 1.3 Hz, 2H), 3.94 (s, 2H). ^{13}C NMR (100 MHz, DMSO-d_6) δ 179.0, 171.6, 171.3, 166.7, 150.8, 147.5, 137.5, 134.3, 133.8, 123.5, 116.4, 46.1.

*(2-(Allylamino)-4-aminothiazol-5-yl)(naphthalen-2-yl)-methanone (**4**).* Yellow solid: mp (EtOAc/MeOH) 178−180 °C. ^{1}H NMR (400 MHz, DMSO-d_6) δ 8.80 (s, 1H), 8.20 (s, 1H), 7.99 (ddd, J = 4.96, 10.61, 19.80 Hz, 3H), 7.73 (dd, J = 1.68, 8.48 Hz, 1H), 7.64−7.53 (m, 2H), 5.88 (ddd, J = 5.18, 10.35, 22.17 Hz, 1H), 5.49 (D, J = 40.52 Hz, 1H), 5.18 (ddd, J = 1.48, 11.66, 13.74 Hz, 2H), 3.93 (s, 2H). ^{13}C NMR (100 MHz, DMSO-d_6) δ 181.5, 166.3, 155.1, 139.5, 133.8, 133.5, 132.1, 128.6, 127.9, 127.6, 127.2, 126.7, 126.1, 124.3, 116.2, 46.1. HRMS calcd for $C_{17}H_{16}N_3O$ S (M + H) 310.1014, found 310.1001.

*(2-(Allylamino)-4-aminothiazol-5-yl)(pyridin-2-yl)methanone (**6**).* Yellow solid: mp (EtOAc/hexane) 178−180 °C. ^{1}H NMR (400 MHz, DMSO-d_6) δ 8.99 (s, 1H), 8.73 (s, 1H), 8.64 (d, J = 4.7 Hz, 1H), 8.10 (d, J = 7.8 Hz, 1H), 7.97−7.95 (m, 2H), 7.55−7.45 (m, 1H), 5.99−5.83 (m, 1H), 5.27−5.12 (m, 2H), 3.99 (d, J = 25.4 Hz, 2H). ^{13}C NMR (100 MHz, DMSO-d_6) δ 175.9, 168.9, 154.9, 147.4, 137.4, 134.1, 125.2, 121.4, 116.0, 45.7.

*(2-(Allylamino)-4-aminothiazol-5-yl)(4-nitrophenyl)methanone (**9**).* Brown solid: mp (EtOAc/MeOH) 183−185 °C. ^{1}H NMR (400 MHz, DMSO-d_6) δ 8.80 (s, 1H), 8.20−7.98 (m, 4H), 7.64−7.51 (m, 2H), 5.88 (ddd, J = 22.2, 10.3, 5.2 Hz, 1H), 5.33−5.06 (m, 2H), 3.93 (s, 2H). ^{13}C NMR (100 MHz, DMSO-d_6) δ 178.9, 167.1, 148.0, 147.7, 133.8, 133.7, 128.0, 123.7, 116.4, 46.2. HRMS calcd for $C_{13}H_{13}N_4O_3$ S (M + H) 305.0708, found 305.0719.

*(2-(Allylamino)-4-aminothiazol-5-yl)(4-chlorophenyl)methanone (**15**).* Yellow solid: mp (EtOAc/hexane) 198−200 °C. ^{1}H NMR (400 MHz, DMSO-d_6) δ 8.84 (br s, 1H), 8.41 (br s, 1H), 7.95 (br s, 1H), 7.64 (ddd, J = 19.8, 10.6, 5.0 Hz, 1H), 7.51 (dd, J = 8.5, 1.7 Hz, 1H), 7.92−7.83 (m, 2H), 5.17 (ddd, J = 22.2, 10.3, 5.2 Hz, 1H), 5.33−5.06 (m, 2H), 3.91 (br s, 2H).

*(4-Amino-2-(phenylamino)thiazol-5-yl)(phenyl)methanone (**16**).* Yellow solid: mp (EtOAc/MeOH) 194−196 °C. ^{1}H NMR (400 MHz, DMSO-d_6) δ 10.78 (s, 1H), 8.21 (s, 2H), 7.76−7.55 (m, 4H), 7.54−7.41 (m, 3H), 7.36 (t, J = 7.8 Hz, 2H), 7.08 (t, J = 7.3 Hz, 1H). ^{13}C NMR (100 MHz, DMSO-d_6) δ 182.7, 167.2, 165.6, 141.9, 139.6, 130.4, 129.1, 128.4, 126.8, 123.4, 119.1.

*(4-Amino-2-(cyclohexylamino)thiazol-5-yl)(phenyl)methanone (**17**).* Yellow solid: mp (EtOAc/MeOH) 181−182 °C. ^{1}H NMR (400 MHz, DMSO-d_6) δ 8.56 (s, 2H), 7.66−7.56 (m, 2H), 7.48−7.38 (m, 3H), 3.59 (s, 1H), 2.16−0.88 (m, 11H). ^{13}C NMR (100 MHz, DMSO-d_6) δ 181.4, 172.3, 166.6, 142.2, 130.0, 128.2, 126.6, 32.1, 25.0, 54.0, 24.4.

*(4-Amino-2-(isopropylamino)thiazol-5-yl)(phenyl)methanone (**18**).* Yellow solid: mp (EtOAc/MeOH) 161−163 °C. ^{1}H NMR (400 MHz, DMSO-d_6) δ 9.07−7.66 (m, 3H), 7.67−7.29 (m, 5H), 3.81 (brs, 1H), 1.17 (d, J = 6.5 Hz, 6H). ^{13}C NMR (100 MHz, DMSO-d_6) δ 181.4, 166.6, 142.2, 130.0, 128.2, 126.6, 46.4, 22.1. HRMS calcd for $C_{13}H_{15}N_3O$ S (M + H) 262.1014, found 262.1014.

*(4-Amino-2-(propylamino)thiazol-5-yl)(phenyl)methanone (**20**).* Yellow solid: mp (EtOAc/hexane) 159−161 °C. ^{1}H NMR (400 MHz, DMSO-d_6) δ 8.63 (s, 1H), 8.56−7.47 (m, 4H), 7.47−7.39 (m, 3H), 3.19 (s, 2H), 1.65−1.45 (m, 2H), 0.88 (t, J = 7.4 Hz, 3H). ^{13}C NMR (100 MHz, DMSO-d_6) δ 181.5, 171.3, 166.6, 142.2, 130.0, 128.2, 126.7, 91.9, 45.8, 21.8, 11.3. HRMS calcd for $C_{13}H_{16}N_3O$ S (M + H) 262.1002, found 262.1014.

*(4-Amino-2-(2-methylallylamino)thiazol-5-yl)(phenyl)-methanone (**21**).* Yellow solid: mp (EtOAc/hexane) 174−176 °C. ^{1}H NMR (400 MHz, DMSO-d_6) δ 8.81 (br s, 2H), 7.63 (d, J = 8.2, 3.5 Hz, 2H), 7.48−7.25 (m, 3H), 4.85 (d, J = 6.4 Hz, 2H), 3.84 (s, 2H), 1.70 (s, 3H). ^{13}C NMR (100 MHz, DMSO-d_6) δ181.7, 166.4, 142.2, 141.1, 130.0, 128.3, 126.7, 111.0, 92.2, 60.0, 49.3, 20.0.

*(4-Amino-2-(4-(trifluoromethylphenyl)amino)thiazol-5-yl)-(phenyl)methanone (**25**).* Yellow solid: mp (EtOAc/MeOH/DMF) 210−212 °C. ^{1}H NMR (400 MHz, DMSO-d_6) δ 11.11 (s, 1H), 8.24 (s, 2H), 7.85 (d, J = 8.6 Hz, 2H), 7.75−7.58 (m, 4H), 7.56−7.42 (m, 3H). ^{13}C NMR (100 MHz, DMSO-d_6) δ 183.2, 166.4, 165.1, 143.0, 141.7, 130.6, 128.4, 126.8, 126.4, 126.3, 125.7, 123.0, 123.0, 122.7, 118.4.

*(4-Amino-2-(cyclohexylamino)thiazol-5-yl)(3-nitrophenyl)-methanone (**26**).* Yellow solid: mp (EtOAc/MeOH) 185−187 °C. ^{1}H NMR (400 MHz, DMSO-d_6) δ 9.13−7.85 (m, 6H), 7.75 (t, J = 8.0 Hz, 1H), 3.72 (s, 1H), 2.12−1.44 (m, 5H), 1.39−1.03 (m, 5H). ^{13}C NMR (100 MHz, DMSO-d_6) δ 177.8, 167.5, 147.6, 143.3, 133.1, 130.2, 124.6, 121.3, 53.0, 32.0, 25.0, 24.3.

*(4-Amino-2-(cyclohexylamino)thiazol-5-yl)(3-methoxyphenyl)-methanone (**27**).* Yellow solid: mp (EtOAc/MeOH) 184−186 °C. ^{1}H NMR (400 MHz, DMSO-d_6) δ 8.56 (s, 3H), 7.34 (t, J = 7.9 Hz, 1H), 7.24−7.06 (m, 2H), 7.01 (dd, J = 8.1, 2.1 Hz, 1H), 3.78 (s, 3H), 1.89 (d, J = 9.5 Hz, 2H), 1.76−1.49 (m, 3H), 1.44−0.92 (m, 6H). ^{13}C NMR (100 MHz, DMSO-d_6) δ 181.0, 166.7, 159.0, 143.6, 129.4, 118.8, 115.8, 111.9, 55.2, 45.7, 32.1, 25.0, 24.4.

*(4-Amino-2-(phenylamino)thiazol-5-yl)(pyridin-3-yl)methanone (**30**).* Yellow solid: mp (EtOAc/MeOH/DMF) 202−204 °C. ^{1}H NMR (400 MHz, DMSO-d_6) δ 10.87 (s, 1H), 8.84 (d, J = 5.7 Hz, 1H), 8.68 (dd, J = 4.8, 1.6 Hz, 1H), 8.30 (s, 2H), 8.09−7.99 (m, 1H), 7.62 (d, J = 7.8 Hz, 2H), 7.51 (ddd, J = 7.8, 4.8, 0.6 Hz, 1H), 7.36 (d, J = 8.0 Hz,

dx.doi.org/10.1021/jm301234k | J. Med. Chem. 2013, 56, 3768−3782

2H), 7.10 (t, J = 7.4 Hz, 1H). ^{13}C NMR (100 MHz, DMSO-d_6) δ 180.1, 167.4, 165.9, 151.1, 147.6, 139.4, 137.3, 134.4, 129.2, 123.6, 123.6, 119.2.

*(4-Amino-2-(phenylamino)thiazol-5-yl)(3-fluorophenyl)-methanone (**32**).* Yellow solid: mp (EtOAc/MeOH/DMF) 189−191 °C. ^{1}H NMR (400 MHz, DMSO-d_6) δ 10.83 (s, 1H), 8.27 (s, 2H), 7.62 (d, J = 8.0 Hz, 2H), 7.54 (dd, J = 12.4, 5.4 Hz, 2H), 7.47−7.28 (m, 4H), 7.10 (t, J = 7.3 Hz, 1H).

*(4-Amino-2-(phenylamino)thiazol-5-yl)(3-nitrophenyl)-methanone (**33**).* Yellow solid: mp (EtOAc/MeOH) 209−211 °C. ^{1}H NMR (400 MHz, DMSO-d_6) ^{1}H NMR δ 10.92 (s, 1H), 8.97−7.95 (m, 5H), 7.79 (t, J = 8.0 Hz, 1H), 7.64 (d, J = 7.9 Hz, 2H), 7.37 (t, J = 7.9 Hz, 2H), 7.10 (t, J = 7.4 Hz, 1H). ^{13}C NMR (100 MHz, DMSO-d_6) δ 179.2, 167.4, 166.5, 147.7, 142.9, 139.4, 133.2, 130.3, 129.6, 125.0, 123.6, 121.4, 119.2.

(4-Amino-2-(phenylamino)thiazol-5-yl)(3-methoxyphenyl)-methanone (34**).* Yellow solid: mp (EtOAc/MeOH/DMF) 194−196 °C. ^{1}H NMR (400 MHz, DMSO-d_6) δ 10.76 (s, 1H), 8.21 (s, 2H), 7.62 (d, J = 7.8 Hz, 2H), 7.44−7.30 (m, 3H), 7.28−7.15 (m, 2H), 7.13−7.01 (m, 2H), 3.80 (s, 3H). ^{13}C NMR (100 MHz, DMSO-d_6) δ 182.3, 167.2, 165.7, 159.1, 143.3, 139.6, 129.6, 129.1, 123.4, 119.1, 119.0, 116.2, 112.1, 55.2. HRMS calcd for $C_{17}H_{16}N_3O_2$ S (M + H) 326.0958, found 326.0957.

*(4-Amino-2-(phenylamino)thiazol-5-yl)(3-chlorophenyl)-methanone (**35**).* Yellow solid: mp (EtOAc/MeOH/DMF) 205−207 °C. ^{1}H NMR (400 MHz, DMSO-d_6) δ 10.83 (s, 1H), 8.28 (s, 2H), 7.75−7.41 (m, 6H), 7.36 (d, J = 7.8 Hz, 2H), 7.09 (t, J = 7.3 Hz, 1H). ^{13}C NMR (100 MHz, DMSO-d_6) δ 180.5, 167.3, 166.0, 143.8, 139.5, 133.2, 130.4, 130.2, 129.1, 126.6, 125.4, 123.5, 119.1.

*(4-Amino-2-(phenylamino)thiazol-5-yl)(3,5-bis(trifluoromethyl)-phenyl)methanone (**36**).* Yellow solid: mp (EtOAc/MeOH) 192−194 °C. ^{1}H NMR (400 MHz, DMSO-d_6) δ 10.93 (br s, 1H), 9.03−7.90 (m, 5H), 7.66 (d, J = 7.9 Hz, 2H), 7.35 (t, J = 7.9 Hz, 2H), 7.08 (t, J = 7.4 Hz, 1H). ^{13}C NMR (100 MHz, DMSO-d_6) δ 178.1, 167.9, 166.8, 143.8, 139.4, 131.0, 130.6, 130.3, 130.0, 129.1, 127.5, 127.2, 124.5, 123.9, 123.6, 121.7, 119.9.

(4-Amino-2-(phenylamino)thiazol-5-yl)(3-(trifluoromethyl)-phenyl)methanone (37**).* Yellow solid: mp (EtOAc/MeOH) 179−181 °C. ^{1}H NMR (400 MHz, DMSO-d_6) δ 10.86 (s, 1H), 8.34 (s, 2H), 7.93 (dd, J = 41.4, 9.3 Hz, 3H), 7.77−7.53 (m, 3H), 7.36 (t, J = 7.6 Hz, 2H), 7.09 (t, J = 7.2 Hz, 1H). ^{13}C NMR (100 MHz, DMSO-d_6) δ 180.3, 167.2, 166.2, 142.6, 139.4, 130.8, 129.8, 129.2, 129.1, 128.9, 126.9, 125.3, 123.5, 123.3, 122.6, 119.1.

*(4-Amino-2-(phenylamino)thiazol-5-yl)(naphthalen-2-yl)-methanone (**40**).* Yellow solid: mp (EtOAc/MeOH/DMF) 191−196 °C. ^{1}H NMR (400 MHz, DMSO-d_6) δ 10.81 (s, 1H), 8.28 (s, 3H), 8.06−7.95 (m, 3H), 7.78 (dd, J = 8.5, 1.7 Hz, 1H), 7.70−7.49 (m, 4H), 7.36 (dd, J = 8.2, 7.7 Hz, 2H), 7.08 (t, J = 7.4 Hz, 1H). ^{13}C NMR (100 MHz, DMSO-d_6) δ 182.6, 167.2, 165.6, 139.6, 139.3, 133.7, 132.1, 129.1, 128.7, 128.1, 127.7, 127.4, 126.8, 126.5, 124.3, 123.4, 119.0.

4-Amino-2-(phenylamino)thiazole-5-carboxamide (41**).* Yellow solid: mp (EtOAc/MeOH) 145−147 °C. ^{1}H NMR (400 MHz, DMSO-d_6) δ 11.54 (s, 1H), 8.03 (s, 1H), 7.72 (s, 1H), 7.44 (ddd, J = 32.2, 11.2, 4.8 Hz, 4H), 7.22 (t, J = 7.3 Hz, 1H), 3.98 (s, 2H).

4-(4-Amino-5-nicotinoylthiazol-2-ylamino)benzamide (43**).* Yellow solid: mp (EtOAc/MeOH/DMF) 229−231 °C. ^{1}H NMR (400 MHz, DMSO-d_6) δ 11.08 (s, 1H), 8.87 (s, 1H), 8.69 (d, J = 3.9 Hz, 1H), 8.35 (s, 2H), 8.13−7.62 (m, 6H), 7.51 (dd, J = 7.4, 5.0 Hz, 1H), 7.31 (s, 1H). ^{13}C NMR (100 MHz, DMSO-d_6) δ 180.5, 167.3, 166.8, 165.7, 151.2, 147.6, 142.0, 137.2, 134.5, 128.7, 123.6, 117.9.

(4-Amino-2-(isopropylamino)thiazol-5-yl)(pyridin-3-yl)-methanone (44**).* Yellow solid: mp (EtOAc/MeOH) 174−176 °C. ^{1}H NMR (400 MHz, DMSO-d_6) δ 8.79 (d, J = 1.8 Hz, 1H), 8.64 (dd, J = 4.8, 1.6 Hz, 2H), 8.37−7.70 (m, 2H), 7.47 (dd, J = 7.8, 4.8 Hz, 1H), 3.85 (s, 1H), 1.17 (d, J = 6.5 Hz, 6H). ^{13}C NMR (100 MHz, DMSO-d_6) δ 178.7, 166.9, 150.7, 147.5, 137.5, 134.3, 123.5, 46.4, 22.1.

(4-Amino-2-(cyclohexylamino)thiazol-5-yl)(pyridin-3-yl)-methanone (45**).* Yellow solid: mp (EtOAc/MeOH) 174−176 °C. ^{1}H NMR (400 MHz, DMSO-d_6) δ 9.23−7.69 (m, 6H), 7.47 (dd, J = 7.8, 4.8 Hz, 1H), 3.68 (s, 1H), 1.93 (t, J = 19.1 Hz, 2H), 1.77−1.42 (m, 3H), 1.41−0.99 (m, 5H). ^{13}C NMR (100 MHz, DMSO-d_6) δ 178.7, 166.9, 150.7, 147.5, 137.6, 134.3, 123.5, 53.08, 32.1, 24.9, 24.4.

*3-(4-Amino-5-nicotinoylthiazol-2-ylamino)benzenesulfonamide (**49**).* Yellow solid: mp (EtOAc/MeOH/DMF) 194−196 °C. ^{1}H NMR (400 MHz, DMSO-d_6) δ 11.63 (s, 1H), 8.99 (d, J = 1.5 Hz, 1H), 8.83 (dd, J = 5.1, 1.1 Hz, 1H), 8.39 (d, J = 8.0 Hz, 2H), 8.15 (s, 1H), 8.02−7.95 (m, 1H), 7.81 (dd, J = 7.8, 5.3 Hz, 1H), 7.66−7.36 (m, 5H). ^{13}C NMR (100 MHz, DMSO-d_6) δ 178.3, 177.9, 167.1, 149.4, 145.0, 144.5, 143.9, 139.9, 138.3, 129.8, 129.3, 125.3, 121.8, 120.3, 115.9. HRMS calcd for $C_{15}H_{14}N_5O_3$ S_2 (M + H) 376.0538, found 376.0549.

4-(4-Amino-5-(2-nitrobenzoyl)thiazol-2-ylamino)-benzenesulfonamide (51**).* Orange solid: mp 250 °C. ^{1}H NMR (400 MHz, DMSO-d_6): δ 11.16 (s, 1H disappear on D_2O shake), 8.17 (brs 2H, overlapping, disappear on D_2O shake), 8.08 (d, J = 8.4 Hz, 1H, overlapping), 7.82 (dt, J = 7.6, 1.2 Hz, 1H), 7.79−7.76 (m, 4H), 7.69 (dt, J = 8.4, 1.6 Hz, 1H D_2O shake), 7.64 (d, J = 7.6 Hz, 1H), 7.30 (s, 2H, disappear on D_2O shake). ^{13}C NMR (100 MHz, DMSO-d_6): δ 180.24, 167.06, 164.89, 146.76, 142.50, 138.35, 137.23, 134.64, 131.29, 128.74, 127.47, 124.99, 118.74, 94.09. LCMS (ESI+) m/z 420.05 (M + H)$^+$. HRMS (ESI+) m/z calcd for $C_{16}H_{14}N_5O_5S_2$ (M + H1)$^+$ 420.0431, found 420.0428.

4-(4-Amino-5-(3-fluorobenzoyl)thiazol-2-ylamino)-benzenesulfonamide (52**).* Yellow solid: mp (EtOAc/MeOH/DMF) 202−204 °C. ^{1}H NMR (400 MHz, DMSO-d_6) δ 11.14 (s, 1H), 8.30 (s, 2H), 7.86−7.75 (m, 4H), 7.59−7.24 (m, 6H). ^{13}C NMR (100 MHz, DMSO-d_6) δ 181.3, 166.6, 165.5, 163.2, 160.7, 144.0, 142.3, 138.1, 130.7, 127.0, 122.9, 118.3, 117.4, 113.8, 113.6.

4-(4-Amino-5-4-(4-Amino-5-(3-aminobenzoyl)thiazol-2-ylamino)benzenesulfonamide (55**).* Yellow solid: mp (EtOAc/MeOH/DMF) 201−203 °C. ^{1}H NMR (400 MHz, DMSO-d_6) δ 11.04 (s, 1H), 8.12 (s, 2H), 7.79 (s, 4H), 7.42−6.47 (m, 6H), 5.31 (s, 2H). ^{13}C NMR (100 MHz, DMSO-d_6) δ 184.2, 166.3, 165.9, 164.7, 148.8, 142.6, 137.8, 128.8, 126.9, 118.1, 115.9, 114.1, 112.0.

4-(4-Amino-5-(3-methoxybenzoyl)thiazol-2-ylamino)-benzenesulfonamide (56**).* Yellow solid: mp (EtOAc/MeOH/DMF) 216−218 °C. ^{1}H NMR (400 MHz, DMSO-d_6) δ 11.10 (s, 1H), 8.65−7.88 (m, 2H), 7.87−7.75 (m, 4H), 7.44−7.14 (m, 5H), 7.08 (dd, J = 8.2, 2.0 Hz, 1H), 3.81 (s, 3H)). ^{13}C NMR (100 MHz, DMSO-d_6) δ 182.8, 166.5, 165.2, 159.2, 143.1, 142.4, 138.0, 129.7, 127.0, 119.0, 118.2, 116.5, 112.1, 55.3.

4-(4-Amino-5-benzoylthiazol-2-ylamino)benzenesulfonamide (57**).* Yellow solid: mp (EtOAc/MeOH/DMF) 218−220 °C. ^{1}H NMR (400 MHz, DMSO-d_6) δ 11.09 (s, 1H), 8.23 (s, 2H), 7.84−7.76 (m, 4H), 7.69 (dd, J = 7.4, 1.5 Hz, 2H), 7.54−7.44 (m, 3H), 7.28 (s, 2H). ^{13}C NMR (100 MHz, DMSO-d_6) δ 183.2, 166.4, 165.1, 142.4, 141.7, 138.0, 130.6, 128.5, 127.0, 126.8, 118.2.

4-(4-Amino-5-(3-(trifluoromethyl)benzoyl)thiazol-2-ylamino)-benzenesulfonamide (58**).* Yellow solid: mp (EtOAc/MeOH/DMF) 220−222 °C. ^{1}H NMR (400 MHz, DMSO-d_6) δ 11.18 (s, 1H), 8.36 (s, 2H), 7.99 (d, J = 8.9 Hz, 2H), 7.89 (d, J = 7.8 Hz, 1H), 7.85−7.68 (m, 5H), 7.28 (s, 2H). ^{13}C NMR (100 MHz, DMSO-d_6) δ 180.9, 166.6, 165.7, 142.4, 142.3, 138.2, 130.9, 129.9, 129.3, 129.0, 127.1, 127.0, 123.4, 123.3, 118.2.

4-(4-Amino-5-(3-chlorobenzoyl)thiazol-2-ylamino)-benzenesulfonamide (65**).* Yellow solid: mp (EtOAc/MeOH/DMF) 210−212 °C. ^{1}H NMR (400 MHz, DMSO-d_6) δ 11.15 (s, 1H), 8.31 (s, 2H), 7.93−7.74 (m, 4H), 7.59 (ddd, J = 36.4, 18.0, 10.4 Hz, 4H), 7.29 (s, 2H). ^{13}C NMR (100 MHz, DMSO-d_6) δ 181.1, 166.6, 165.6, 143.6, 142.3, 138.1, 133.3, 130.5, 130.4, 127.0, 126.7, 125.5, 118.3.

4-(4-Amino-5-(4-methoxybenzoyl)thiazol-2-ylamino)-benzenesulfonamide (66**).* Yellow solid: mp (EtOAc/MeOH/DMF) 217−219 °C. ^{1}H NMR (400 MHz, DMSO-d_6) δ 11.07 (s, 1H), 8.17 (s, 2H), 7.88−7.74 (m, 4H), 7.70 (d, J = 8.7 Hz, 2H), 7.28 (s, 2H), 7.03 (d, J = 8.7 Hz, 2H), 3.82 (s, 3H). ^{13}C NMR (100 MHz, DMSO-d_6) δ 182.5, 166.0, 164.9, 161.1, 142.5, 137.9, 134.0, 128.9, 127.0, 118.1, 113.7, 55.3.

*4-(4-Amino-5-(3,5-bis(trifluoromethyl)benzoyl)thiazol-2-ylamino)benzenesulfonamide (**67**).* Yellow solid: mp (EtOAc/MeOH/DMF) 224−226 °C. ^{1}H NMR (400 MHz, DMSO-d_6) δ 11.25 (s, 1H), 8.46 (s, 2H), 8.30 (d, J = 9.2 Hz, 3H), 7.82 (q, J = 9.0 Hz, 4H), 7.30 (s, 2H). ^{13}C NMR (100 MHz, DMSO-d_6) δ 178.8,

166.7, 166.2, 143.6, 142.2, 138.3, 131.0, 130.7, 130.4, 130.0, 127.6, 127.2, 127.0, 124.5, 124.1, 121.7, 118.3. HRMS calcd for $C_{18}H_{12}F_6N_4O_3S_2$ (M + H) 511.0335, found 511.0336.

*4-(5-(2-Naphthoyl)-4-aminothiazol-2-ylamino)-benzenesulfonamide (**69**). Yellow solid: mp (EtOAc/MeOH/DMF) 220−222 °C. ^{1}H NMR (400 MHz, DMSO-d_6) δ 11.13 (s, 1H), 8.31 (s, 3H), 8.01 (ddd, J = 13.1, 9.0, 6.7 Hz, 3H), 7.86−7.75 (m, 5H), 7.65−7.56 (m, 2H), 7.29 (s, 2H). ^{13}C NMR (100 MHz, DMSO-d_6) δ 183.3, 166.7, 165.4, 142.7, 139.3, 138.2, 134.0, 132.3, 129.0, 128.4, 127.9, 127.7, 127.2, 127.1, 126.9, 124.5, 118.4.

3-(4-Amino-5-(3-fluorobenzoyl)thiazol-2-ylamino)-benzenesulfonamide (**83**). Yellow solid: mp (EtOAc/MeOH/DMF) 182−184 °C. ^{1}H NMR (400 MHz, DMSO-d_6) δ 11.08 (s, 1H), 8.27 (s, 2H), 8.07 (s, 1H), 7.96 (d, J = 7.2 Hz, 1H), 7.69−7.22 (m, 8H).

4-Amino-N-(4-nitrophenyl)-2-(4-sulfamoylphenylamino)-thiazole-5-carboxamide (**93**). Yellow solid: mp (EtOAc/MeOH) 228−230 °C. ^{1}H NMR (400 MHz, DMSO-d_6) δ 10.99 (s, 1H), 9.62 (s, 1H), 8.17 (d, J = 8.9 Hz, 2H), 7.93 (d, J = 9.0 Hz, 2H), 7.87−7.64 (m, 4H), 7.33 (d, J = 47.4 Hz, 4H). ^{13}C NMR (100 MHz, DMSO-d_6) δ 163.7, 163.6, 162.7, 146.6, 142.9, 141.3, 137.5, 127.0, 124.6, 119.2, 117.7.

Enzyme Assays. The synthetic peptide PKTPKKAKKL[42] served as a substrate for the activated CDK2−cyclin A2 complex, and the formation of ADP from ATP was coupled to the oxidation of NADH using pyruvate kinase (PK) and lactate dehydrogenase (LDH), monitored at 340 nm.[43,44] Assays for the HTS campaign (Z-factor = 0.74) and dose−response measurements for SAR were carried out in 384-well plates at room temperature in 50 mM Tris-HCl buffer (pH 7.5) containing 10 mM $MgCl_2$, 0.24 mM NADH, 5 mM DTT, 6 U mL^{-1} LDH, 10 U mL^{-1} PK, 1 mM phosphoenolpyruvate, 5% (v/v) DMSO, and 0.15 μM (0.01 mg mL^{-1}) activated CDK−cyclin A2 complex. Inhibitor was added to the mixture, and the reaction was initiated by the addition of 0.2 mM ATP and 0.125 mM peptide substrate. The more sensitive ADP Quest fluorescence assay (DiscoveRx, Fremont, CA)[45] was employed for compounds with IC_{50} values below 1.0 μM. In this assay, the formation of ADP is coupled to the generation of a fluorescent resorufin dye (excitation and emission wavelengths of 540 and 590 nm, respectively). Reactions were carried out at room temperature in 15 mM HEPES buffer (pH 7.4) containing 20 mM NaCl, 1 mM EGTA, 0.02% Tween 20, 10 mM $MgCl_2$, 5% (v/v) DMSO, and 8.8 nM (0.56 μg mL^{-1}) activated CDK2−cyclin A2. Inhibitor was added to the mixture, and the reaction was initiated by the addition of 150 μM ATP and 100 μM peptide substrate. All kinetic assays were performed in 384-well plates using a Wallac Envision 2102 plate reader (Perkin-Elmer). IC_{50} values were obtained by fitting data to eq 1, where A is the fraction of activity remaining, $[I]$ is the concentration of inhibitor, and n is the Hill slope coefficient.

$$A = \frac{1}{1 + \left(\frac{[I]}{IC_{50}}\right)^n} \quad (1)$$

The most potent compounds, **42** and **51**, were further analyzed by Reaction Biology Corporation (Malvern, PA) using a highly sensitive P^{33}-radiolabeled assay against CDK2−cyclin A2.

Kinase Profiling. Selected compounds were tested against a panel of 48 kinases provided by Caliper Life Sciences (Hopkinton, MA), which is representative of the entire human kinome. This kinase panel, available as ProfilerPro Kits 1 and 2, was tested using a Caliper LC3000 instrument in an electrophoretic mobility-shift assay at the High Throughput Screening Laboratory in the Institute for Therapeutics Discovery and Development at the University of Minnesota, College of Pharmacy. Compounds were added to the plates and preincubated with enzyme for 15 min, followed by addition of peptide substrates and ATP for a 90 min reaction period at 28 °C. Inhibitory activity was determined by measuring the conversion of nonphosphorylated peptide substrate to phosphorylated product, expressed relative to plate controls. The Spotfire visualization program (Tibco Software, Palo Alto, CA) was used to generate a gradient heat map of the inhibitory activities (Figure S3 of Supporting Information). The profiling of compound **51** against a panel of 339 kinases and the dose−response kinetics against different CDK−cyclin complexes were performed by Reaction Biology Corp. using a P^{33}-radiolabeled assay. Residual enzymatic activity (in % of DMSO controls) was determined in duplicate at a compound concentration of 0.1 μM for the profiling and between 0.05 nM and 1000 nM for the dose−response analysis; the ATP concentration was 10 μM and staurosporine served as a positive control.

X-ray Crystallography. Crystallization was performed at 19 °C using the hanging drop vapor diffusion method. Crystals of CDK2−inhibitor complexes were grown from a solution of 10 mg mL^{-1} CDK2 in the presence of 0.5−3 mM compound with 0.1 M HEPES/NaOH (pH 7.5) and 10% (v/v) polyethylene glycol 3350. Crystals were harvested in cryoprotectant (50 mM HEPES pH 7.5, 50 mM phosphate (Na/K) pH 7.5, 15% (v/v) polyethylene glycol 3350, 23% (v/v) ethylene glycol, and 0.5 mM inhibitor) prior to data collection. X-ray diffraction data were recorded at −180 °C in the Moffitt Cancer Center Chemical Biology Core using the rotation method on single crystals (Cu Kα radiation generated by Rigaku Micro-Max 007-HF, equipped with an HTC image plate and a Rigaku CCD Saturn 944 detector). The data set for compound **51** was recorded at the APS (Argonne National Laboratories) beamline 22-ID (SER-CAT) at a wavelength of 1.0 Å. Data were reduced with XDS[46] or HKL-2000.[47] CNS[48] was employed for phasing and refinement (minimization and simulated annealing), and model building was performed using O[49] or Coot.[50] Initial models for the inhibitors were generated using Chem3DPro (CambridgeSoft), and parameter and topology files were generated using xplo2d.[51] Figures were drawn with PyMol (Schrödinger, Inc.). Data and refinement statistics are shown in the Supporting Information (Table S1), along with the $F_o - F_c$ electron density maps from refinement cycles omitting the respective ligands (Figure S5 of Supporting Information).

Cell Viability Assays. Cell lines were obtained from the American Type Culture Collection (Manassas, VA) and maintained in RPMI or DMEM with 10% fetal bovine serum, 37 °C, and 5% CO_2. All cell lines tested free of mycoplasma with MycoAlert tests (Lonza Rockland, Inc., Rockland, ME), and the cell line identities were confirmed using StemElite ID system (Promega Corp., Madison, WI).

For viability assays using MTT (3-(4,5-dimethythiazol-2-yl)-2,5-diphenyltetrazolium bromide), cells were plated in 96-well plates in 100 μL of medium and were allowed to attach overnight. Cells were then incubated for 72 h with increasing concentrations of inhibitor. Media was aspirated and replaced with 100 μL of complete media containing 1 mg mL^{-1} MTT ((3-(4,5-dimethythiazol-2-yl)-2,5-diphenyltetrazolium bromide) and incubated for 3 h at 37 °C in 5% CO_2 humidified incubator. Media was then aspirated, and DMSO was added. Cells were incubated for 10 min at room temperature while shaking, and optical density was determined at 540 nm using a μQuant spectrophotometric plate reader (Bio-TEK, Winooski, VT). NCI-H929 and U266 cells were cultured in RPMI-1640 media (GIBCO, Life Technologies Carlsbad, CA), supplemented with 10% fetal bovine serum (GIBCO) including 0.05 mM 2-mercaptoethanol for NCI-H929 cells. Cells were plated in 96-well plate at a density of 10×10^3 cells/well. MTT assays with GC-1, GC-2, and TM-4 testis cells were carried out as above, with modifications in culture conditions as appropriate for these cell lines.[52−54]

For viability assays using high-throughput CellTiter-Blue, 1200 cells were plated in each well of 384-well plates using a Precision XS liquid handling station (Bio-Tek Instruments, Inc., Winooski, VT) and allowed to incubate overnight at 37 °C and 5% CO_2. A liquid handling station was used to serially dilute all drugs (2:3) in media, and 6 μL of these dilutions were added to appropriate wells. Four replicate wells were used for each drug concentration, and an additional four control wells received a diluent control without drug. After a 72 h incubation period with drugs, 5 μL of CellTiter-Blue reagent (Promega Corp.) were added to each well. Cell viability was assessed by the ability of the remaining viable cells to reduce resazurin to resorufin. The fluorescence of resorufin (579 nm excitation/584 nm emission) was measured with a Synergy 4 microplate reader (Bio-Tek Instruments, Inc.). The fluorescence data were transferred to Microsoft Excel to

dx.doi.org/10.1021/jm301234k | J. Med. Chem. 2013, 56, 3768−3782

calculate the percent viability relative to the four replicate cell wells that did not receive drug. IC_{50} values were determined using a sigmoidal equilibrium model regression using XLfit version 5.2 (ID Business Solutions Ltd.).

Assessment of Activated Caspase. Caspase 3/7 activation was measured using a plate-based Caspase-Glo 3/7 (Promega) luminescent assay. Cells were plated to white 384-well plates as described for cell viability assays. Cells were treated for 24 h with serial dilutions of each compound. For the detection of cleaved caspase-3, H929 cells were plated at a density of 4×10^5 cells/mL and treated with DMSO control, 1.5 μM compound **51**, or 0.005 μM dinaciclib for 24 h. Cleaved caspase-3 levels were assessed using the mAb FITC Active caspase-3 apoptosis kit (BD Pharmingen). Samples were analyzed using a FACScan flow cytometer (BD Biosciences). The experiment was performed in triplicate.

Immunoblotting. A-673 cells were grown to ~70% confluence, and compounds were added. After exposure to the compounds for 24 h, the cells were lysed in cell lysis buffer (Cell Signaling, Danvers, MA). The soluble protein concentration was determined using the Bio-Rad Protein Assay reagent, and 50 μg of total protein wad loaded on each lane of a 10% SDS-polyacrylamide gel. The proteins were then transferred to nitrocellulose membrane, washed with TBS/0.1% Tween 20, and incubated in 1× TBS−Tween20/2% BSA overnight at 4 °C with primary antibodies. Antibody for phospho-Rb (Ser807/811, no. 9308) was obtained from Cell Signaling. β-Actin (clone AC-74) antibody was obtained from Sigma-Aldrich (St. Louis, MO; no. A2228). The membrane was then washed with TBS/0.1% Tween 20, incubated for 1 h at room temperature with goat antimouse 800 nm fluorescent and goat antirabbit 680 nm fluorescent labeled antibodies, and scanned on a Li-Cor (Lincoln, NE) Odyssey infrared scanner. H929 cells were plated at a density of 4×10^5 cells/mL. After treatment for 24 h, cells were washed with cold PBS and lysed in 100 μL of RIPA lysis buffer (Upstate, Lake Placid, NY). Then 10 μg of total protein was loaded on an 8% SDS-PAGE gel. Proteins were resolved by electrophoresis, transferred to a polyvinylidene fluoride (PVDF) membrane, and then blocked overnight in 5% nonfat milk in TBS-0.05% Tween-20. Protein levels were examined with antisera specific antibodies to pRb (Ser807/811) or GAPDH (Cell Signaling, Beverly, MA) and visualized with chemoluminescence (Pierce, Rockford, IL).

■ ASSOCIATED CONTENT

Ⓢ Supporting Information

X-ray crystallography data and refinement statistics, $F_o - F_c$ electron density omit maps, additional SAR data along with dose−response graphs, kinase profiling results, and NMR spectra. This material is available free of charge via the Internet at http://pubs.acs.org.

Accession Codes

The atomic coordinates and structure factors for the crystal structures determined as part of this work have been deposited in the Protein Data Bank (entries 3QQK, 3R8V, 3QTQ, 3R8U, 3S00, 3S0O, 3R8Z, 3QTR, 3RJC, 3R9N, 3RAH, 3QTW, 3QTS, 3RPR, 3RZB, 3QU0, 3RK7, 3RK9, 3RKB, 3RK5, 3QXP, 3QTZ, 3QTU, 3QTX, 3RPV, 3RAL, 3RAK, 3RPY, 3SQQ, 3S1H, 3RMF, 3RNI, 3R9D, 3R9O, 3R9H, and 4GCJ).

■ AUTHOR INFORMATION

Corresponding Author

*For E.S: phone, +813-745-4503; e-mail, ernst.schonbrunn@moffitt.org. For G.I.G.: phone, +612-626-6320; e-mail, georg@umn.edu.

Notes

The authors declare no competing financial interest.

■ ACKNOWLEDGMENTS

We thank the Moffitt Core facilities Chemical Biology, Translational Research, and Flow Cytometry for assistance in X-ray data collection and cell biological studies. We acknowledge the technical support of Nestor Rodriguez, Anne Hoffman, and Todd Hall (University of Kansas Medical School) for performing MTT assays on testis cell lines. We thank Drs. Bi-Cheng Wang and Lirong Chen (SER-CAT, University of Georgia) for support during Synchrotron data collection at Argonne National Laboratory. We thank Katinka Baehr (University of Kansas) for assistance with the production of CDK2-cyclin A, and Dr. Subhashree Francis (University of Minnesota) for assistance with mass spectrometry analysis of compounds. We thank Donna J. Ingles (Moffitt) for help with the preparation of the manuscript and Dr. Jin-Yi Zhu for assistance with X-ray data collection. This work was supported by the Contraceptive Discovery and Development Branch of the *Eunice Kennedy Shriver* National Institute of Child Health and Human Development through contract HHSN275200503400C (N01-HD-5-3400). We thank program officers Drs. H. K. Kim, Diana Blithe, and Min Lee for their support of this project.

■ ABBREVIATIONS USED

CAK, CDK-activating kinase; DMEM, Dulbecco's Modified Eagle's Medium; EGTA, ethylene glycol tetraacetic acid; HEPES, 4-(2-hydroxyethyl)-1-piperazineethanesulfonic acid; HTS, high throughput screening; LDH, lactate dehydrogenase; MTT, 3-(4,5-dimethylthiazol-2-yl)-2,5-diphenyltetrazolium bromide; PK, pyruvate kinase; SAR, structure−activity relationship

■ REFERENCES

(1) Johnson, L. N. Protein kinase inhibitors: contributions from structure to clinical compounds. *Q. Rev. Biophys.* **2009**, *42*, 1−40.
(2) Hall, M.; Peters, G. Genetic alterations of cyclins, cyclin-dependent kinases, and Cdk inhibitors in human cancer. *Adv. Cancer. Res.* **1996**, *68*, 67−108.
(3) Grana, X.; Reddy, E. P. Cell cycle control in mammalian cells: role of cyclins, cyclin dependent kinases (CDKs), growth suppressor genes and cyclin-dependent kinase inhibitors (CKIs). *Oncogene* **1995**, *11*, 211−219.
(4) Morgan, D. O. Principles of CDK regulation. *Nature* **1995**, *374*, 131−134.
(5) Sherr, C. J. Cancer cell cycles. *Science* **1996**, *274*, 1672−1777.
(6) Weinberg, R. A. The retinoblastoma protein and cell cycle control. *Cell* **1995**, *81*, 323−330.
(7) van den Heuvel, S.; Harlow, E. Distinct roles for cyclin-dependent kinases in cell cycle control. *Science* **1993**, *262*, 2050−2054.
(8) Fu, W.; Ma, L.; Chu, B.; Wang, X.; Bui, M. M.; Gemmer, J.; Altiok, S.; Pledger, W. J. The cyclin-dependent kinase inhibitor SCH 727965 (dinaciclib) induces the apoptosis of osteosarcoma cells. *Mol. Cancer Ther.* **2011**, *10*, 1018−1027.
(9) Malumbres, M.; Barbacid, M. To cycle or not to cycle: a critical decision in cancer. *Nature Rev. Cancer* **2001**, *1*, 222−231.
(10) Horiuchi, D.; Huskey, N. E.; Kusdra, L.; Wohlbold, L.; Merrick, K. A.; Zhang, C.; Creasman, K. J.; Shokat, K. M.; Fisher, R. P.; Goga, A. Chemical-genetic analysis of cyclin dependent kinase 2 function reveals an important role in cellular transformation by multiple oncogenic pathways. *Proc. Natl. Acad. Sci. U. S. A.* **2012**, *109*, 1019−1027.
(11) Ortega, S.; Prieto, I.; Odajima, J.; Martin, A.; Dubus, P.; Sotillo, R.; Barbero, J. L.; Malumbres, M.; Barbacid, M. Cyclin-dependent kinase 2 is essential for meiosis but not for mitotic cell division in mice. *Nature Genet.* **2003**, *35*, 25−31.

(12) van der Meer, T.; Chan, W. Y.; Palazon, L. S.; Nieduszynski, C.; Murphy, M.; Sobczak-Thepot, J.; Carrington, M.; Colledge, W. H. Cyclin A1 protein shows haplo-insufficiency for normal fertility in male mice. *Reproduction* **2004**, *127*, 503−511.
(13) Yang, R.; Muller, C.; Huynh, V.; Fung, Y. K.; Yee, A. S.; Koeffler, H. P. Functions of cyclin A1 in the cell cycle and its interactions with transcription factor E2F-1 and the Rb family of proteins. *Mol. Cell. Biol.* **1999**, *19*, 2400−2407.
(14) Nya-Ngatchou, J. J.; Amory, J. K. New approaches to male non-hormonal contraception. *Contraception* **2013**, *87*, 296−299.
(15) Page, S. T.; Amory, J. K.; Bremner, W. J. Advances in male contraception. *Endocr. Rev.* **2008**, *29*, 465−493.
(16) Tash, J. S.; Attardi, B.; Hild, S. A.; Chakrasali, R.; Jakkaraj, S. R.; Georg, G. I. A novel potent indazole carboxylic acid derivative blocks spermatogenesis and is contraceptive in rats after a single oral dose. *Biol. Reprod.* **2008**, *78*, 1127−1138.
(17) Cicenas, J.; Valius, M. The CDK inhibitors in cancer research and therapy. *J. Cancer. Res. Clin. Oncol.* **2011**, *137*, 1409−1418.
(18) Massard, C.; Soria, J. C.; Anthoney, D. A.; Proctor, A.; Scaburri, A.; Pacciarini, M. A.; Laffranchi, B.; Pellizzoni, C.; Kroemer, G.; Armand, J. P.; Balheda, R.; Twelves, C. J. A first in man, phase I dose-escalation study of PHA-793887, an inhibitor of multiple cyclin-dependent kinases (CDK2, 1 and 4) reveals unexpected hepatotoxicity in patients with solid tumors. *Cell Cycle* **2011**, *10*, 963−970.
(19) Guha, M. Cyclin-dependent kinase inhibitors move into Phase III. *Nature Rev. Drug Discovery* **2012**, *11*, 892−894.
(20) Guha, M. Blockbuster dreams for Pfizer's CDK inhibitor. *Nature Biotechnol.* **2013**, *31*, 187.
(21) Paruch, K.; Dwyer, M. P.; Alvarez, C.; Brown, C.; Chan, T.-Y.; Doll, R. J.; Keertikar, K.; Knutson, C.; McKittrick, B.; Rivera, J.; Rossman, R.; Tucker, G.; Fischmann, T.; Hruza, A.; Madison, V.; Nomeir, A. A.; Wang, Y.; Kirschmeier, P.; Lees, E.; Parry, D.; Sgambellone, N.; Seghezzi, W.; Schultz, L.; Shanahan, F.; Wiswell, D.; Xu, X.; Zhou, Q.; James, R. A.; Paradkar, V. M.; Park, H.; Rokosz, L. R.; Stauffer, T. M.; Guzi, T. J. Discovery of Dinaciclib (SCH 727965): A Potent and Selective Inhibitor of Cyclin-Dependent Kinases. *ACS Med. Chem. Lett.* **2010**, *1*, 204−208.
(22) Parry, D.; Guzi, T.; Shanahan, F.; Davis, N.; Prabhavalkar, D.; Wiswell, D.; Seghezzi, W.; Paruch, K.; Dwyer, M. P.; Doll, R.; Nomeir, A.; Windsor, W.; Fischmann, T.; Wang, Y.; Oft, M.; Chen, T.; Kirschmeier, P.; Lees, E. M. Dinaciclib (SCH 727965), a novel and potent cyclin-dependent kinase inhibitor. *Mol. Cancer Ther.* **2010**, *9*, 2344−2353.
(23) Toogood, P. L.; Harvey, P. J.; Repine, J. T.; Sheehan, D. J.; VanderWel, S. N.; Zhou, H.; Keller, P. R.; McNamara, D. J.; Sherry, D.; Zhu, T.; Brodfuehrer, J.; Choi, C.; Barvian, M. R.; Fry, D. W. Discovery of a potent and selective inhibitor of cyclin-dependent kinase 4/6. *J. Med. Chem.* **2005**, *48*, 2388−2406.
(24) Matthews, T. P.; Klair, S.; Burns, S.; Boxall, K.; Cherry, M.; Fisher, M.; Westwood, I. M.; Walton, M. I.; McHardy, T.; Cheung, K. M.; Van Montfort, R.; Williams, D.; Aherne, G. W.; Garrett, M. D.; Reader, J.; Collins, I. Identification of inhibitors of checkpoint kinase 1 through template screening. *J. Med. Chem.* **2009**, *52*, 4810−4819.
(25) Getlik, M.; Grutter, C.; Simard, J. R.; Nguyen, H. D.; Robubi, A.; Aust, B.; van Otterlo, W. A.; Rauh, D. Structure-based design, synthesis and biological evaluation of *N*-pyrazole, *N*′-thiazole urea inhibitors of MAP kinase p38alpha. *Eur. J. Med. Chem.* **2012**, *48*, 1−15.
(26) Vulpetti, A.; Casale, E.; Roletto, F.; Amici, R.; Villa, M.; Pevarello, P. Structure-based drug design to the discovery of new 2-aminothiazole CDK2 inhibitors. *J. Mol. Graphics Modell.* **2006**, *24*, 341−348.
(27) Ahn, J. S.; Radhakrishnan, M. L.; Mapelli, M.; Choi, S.; Tidor, B.; Cuny, G. D.; Musacchio, A.; Yeh, L. A.; Kosik, K. S. Defining Cdk5 ligand chemical space with small molecule inhibitors of tau phosphorylation. *Chem. Biol.* **2005**, *12*, 811−823.
(28) Helal, C. J.; Sanner, M. A.; Cooper, C. B.; Gant, T.; Adam, M.; Lucas, J. C.; Kang, Z.; Kupchinsky, S.; Ahlijanian, M. K.; Tate, B.; Menniti, F. S.; Kelly, K.; Peterson, M. Discovery and SAR of 2-aminothiazole inhibitors of cyclin-dependent kinase 5/p25 as a potential treatment for Alzheimer's disease. *Bioorg. Med. Chem. Lett.* **2004**, *14*, 5521−5525.
(29) Laha, J. K.; Zhang, X.; Qiao, L.; Liu, M.; Chatterjee, S.; Robinson, S.; Kosik, K. S.; Cuny, G. D. Structure−activity relationship study of 2,4-diaminothiazoles as Cdk5/p25 kinase inhibitors. *Bioorg. Med. Chem. Lett.* **2011**, *21*, 2098−2101.
(30) Anastassiadis, T.; Deacon, S. W.; Devarajan, K.; Ma, H.; Peterson, J. R. Comprehensive assay of kinase catalytic activity reveals features of kinase inhibitor selectivity. *Nature Biotechnol.* **2011**, *29*, 1039−1045.
(31) Jeffrey, P. D.; Russo, A. A.; Polyak, K.; Gibbs, E.; Hurwitz, J.; Massague, J.; Pavletich, N. P. Mechanism of CDK activation revealed by the structure of a cyclinA−CDK2 complex. *Nature* **1995**, *376*, 313−320.
(32) Steuber, H.; Heine, A.; Klebe, G. Structural and thermodynamic study on aldose reductase: nitro-substituted inhibitors with strong enthalpic binding contribution. *J. Mol. Biol.* **2007**, *368*, 618−638.
(33) Lesuisse, D.; Dutruc-Rosset, G.; Tiraboschi, G.; Dreyer, M. K.; Maignan, S.; Chevalier, A.; Halley, F.; Bertrand, P.; Burgevin, M. C.; Quarteronet, D.; Rooney, T. Rational design of potent GSK3beta inhibitors with selectivity for Cdk1 and Cdk2. *Bioorg. Med. Chem. Lett.* **2010**, *20*, 1985−1989.
(34) Echalier, A.; Endicott, J. A.; Noble, M. E. Recent developments in cyclin-dependent kinase biochemical and structural studies. *Biochim. Biophys. Acta* **2010**, *1804*, 511−519.
(35) Sirianni, R.; Chimento, A.; Ruggiero, C.; De Luca, A.; Lappano, R.; Ando, S.; Maggiolini, M.; Pezzi, V. The novel estrogen receptor, G protein-coupled receptor 30, mediates the proliferative effects induced by 17beta-estradiol on mouse spermatogonial GC-1 cell line. *Endocrinology* **2008**, *149*, 5043−5051.
(36) Chen, H.; Fok, K. L.; Jiang, X.; Jiang, J.; Chen, Z.; Gui, Y.; Chan, H. C.; Cai, Z. CD147 regulates apoptosis in mouse spermatocytes but not spermatogonia. *Hum. Reprod.* **2012**, *27*, 1568−1576.
(37) McKee, C. M.; Ye, Y.; Richburg, J. H. Testicular germ cell sensitivity to TRAIL-induced apoptosis is dependent upon p53 expression and is synergistically enhanced by DR5 agonistic antibody treatment. *Apoptosis* **2006**, *11*, 2237−2250.
(38) Robillard, K. R.; Hoque, T.; Bendayan, R. Expression of ATP-binding cassette membrane transporters in rodent and human sertoli cells: relevance to the permeability of antiretroviral therapy at the blood−testis barrier. *J. Pharmacol. Exp. Ther.* **2012**, *340*, 96−108.
(39) Musa, F. R.; Tokuda, M.; Kuwata, Y.; Ogawa, T.; Tomizawa, K.; Konishi, R.; Takenaka, I.; Hatase, O. Expression of cyclin-dependent kinase 5 and associated cyclins in Leydig and Sertoli cells of the testis. *J. Androl.* **1998**, *19*, 657−666.
(40) T'Ang, A.; Varley, J. M.; Chakraborty, S.; Murphree, A. L.; Fung, Y. K. Structural rearrangement of the retinoblastoma gene in human breast carcinoma. *Science* **1988**, *242*, 263−266.
(41) Betzi, S.; Alam, R.; Martin, M. P.; Lubbers, D. J.; Han, H.; Jakkaraj, S. R.; Georg, G. I.; Schonbrunn, E. Discovery of a potential allosteric ligand binding site in CDK2. *ACS Chem. Biol.* **2011**, *6*, 492−501.
(42) Stevenson-Lindert, L. M.; Fowler, P.; Lew, J. Substrate specificity of CDK2-cyclin A. What is optimal? *J. Biol. Chem.* **2003**, *278*, 50956−50960.
(43) Adams, J. A.; McGlone, M. L.; Gibson, R.; Taylor, S. S. Phosphorylation modulates catalytic function and regulation in the cAMP-dependent protein kinase. *Biochemistry* **1995**, *34*, 2447−2454.
(44) Cook, P. F.; Neville, M. E., Jr.; Vrana, K. E.; Hartl, F. T.; Roskoski, R., Jr. Adenosine cyclic 3′,5′-monophosphate dependent protein kinase: kinetic mechanism for the bovine skeletal muscle catalytic subunit. *Biochemistry* **1982**, *21*, 5794−5799.
(45) Martin, M. P.; Zhu, J. Y.; Lawrence, H. R.; Pireddu, R.; Luo, Y.; Alam, R.; Ozcan, S.; Sebti, S. M.; Lawrence, N. J.; Schonbrunn, E. A novel mechanism by which small molecule inhibitors induce the DFG flip in Aurora A. *ACS Chem. Biol.* **2012**, *7*, 698−706.
(46) Kabsch, W. Automatic processing of rotation diffraction data from crystals of initially unknown symmetry and cell constants. *J. Appl. Crystallogr.* **1993**, *26*, 795−800.

(47) Otwinowski, Z.; Minor, W. Processing of X-Ray Diffraction Data Collected in Oscillation Mode. *Methods Enzymol.* **1997**, *276*, 307−326.
(48) Brunger, A. T.; Adams, P. D.; Clore, G. M.; DeLano, W. L.; Gros, P.; Grosse-Kunstleve, R. W.; Jiang, J. S.; Kuszewski, J.; Nilges, M.; Pannu, N. S.; Read, R. J.; Rice, L. M.; Simonson, T.; Warren, G. L. Crystallography & NMR system: A new software suite for macromolecular structure determination. *Acta Crystallogr., Sect. D: Biol. Crystallogr.* **1998**, *54*, 905−921.
(49) Jones, T. A.; Zou, J. Y.; Cowan, S. W.; Kjeldgaard, M. Improved methods for building protein models in electron density maps and the location of errors in these models. *Acta. Crystallogr., Sect. A: Found. Crystallogr.* **1991**, *47*, 110−119.
(50) Emsley, P.; Cowtan, K. Coot: model-building tools for molecular graphics. *Acta. Crystallogr., Sect. D: Biol. Crystallogr.* **2004**, *60*, 2126−2132.
(51) Kleywegt, G. J.; Zou, J.-Y.; Kjeldgaard, M.; Jones, T. A. Around, O Crystallography of biological macromolecules. In *International Tables for Crystallography*; Rossmann, M. G.; Arnold, E., Eds.; International Union of Crystallography: Chester, UK, 2001; Vol. *F*, pp 353−356.
(52) Carson, D. D.; Rosenberg, L. I.; Blaner, W. S.; Kato, M.; Lennarz, W. J. Synthesis and secretion of a novel binding protein for retinol by a cell line derived from Sertoli cells. *J. Biol. Chem.* **1984**, *259*, 3117−3123.
(53) Lee, D. Y.; Lee, S. S.; Joo, W. A.; Lee, E. J.; Kim, C. W. Analysis of differentially regulated proteins in TM4 cells treated with bisphenol A. *Biosci. Biotechnol. Biochem.* **2004**, *68*, 1201−1208.
(54) Lizama, C.; Ludwig, A.; Moreno, R. D. Etoposide induces apoptosis and upregulation of TACE/ADAM17 and ADAM10 in an in vitro male germ cell line model. *Biochim. Biophys. Acta* **2011**, *1813*, 120−128.